The Impact of Increased Grid Resolution on the Mixed Layer Depth Variability in the South Atlantic Ocean and Southern Ocean.

A thesis submitted in partial fulfilment of MSc Degree

Department of Oceanography
University of Cape Town

Tania Carol Williams

WLLTAN010

Supervisor: Associate Professor Marcello Vichi

Abstract

The Southern Ocean plays a major role in global climate system. An understanding of Southern Ocean dynamics allows for a better understanding of the carbon cycle and possible future climate conditions. Earth System Models are used to study Southern Ocean dynamics and are currently producing reliable global annual carbon uptake but have limiting seasonal abilities. These models produce dependable results on a global scale, with more conflicting results on a basin scale. Here we study the impact of mesoscale variability on the Mixed Layer Depth in the Sub-Tropical and Sub-Antarctic Zone of the South Atlantic. The region is hugely impacted by the mesoscale variability as a result of the South African boundary currents. We use two regional simulations both at 1/4^{o} resolution, with one model containing online nested child domain over the South African boundary currents (1/12^{o} resolution). The inter-annual simulations both use the same forcing which allow for a comparison study between the two models. Both the nested and standalone model are able to capture the large scale oceanographic features in the domain. The biggest difference is seen in the Agulhas Current region, where the nested model simulates better mesoscale features, resulting in a fairly accurate position of the Agulhas retroflection and return current. The standalone model contains a high temperature and salinity bias which influences the vertical structure of the water column. Both models are able to simulate the seasonality of the MLD in the Sub-Tropical and Sub-Antarctic Zone in the Atlantic sector. The models overestimate MLD in regions closer to the boundary currents. In the nested model the presence of increased mesoscale features promotes stratification of the water column. The differences seen in the MLD of the two models are linked to the temperature and salinity bias in the standalone model as well as the increased mesoscale variability in the nested model.

Acknowledgements

I was lucky enough to have a great supervisor for my MSc, thank you Ass. Prof Marcello Vichi. You were patient, even when I made silly mistakes and you put up with my clutter during our meetings. Thanks to you I will never again forget to add colour bars to my plots. I definitely learnt a lot this year, from both the project and from you.

I would also like to thank Serena, Emeline and Ben for the help with the modelling portion of the project. To Ass. Prof Isabelle Ansorge I would like to say thank you for all the support and motivation throughout the year.

To my class mates, Khush, Tharone, Marc and Rams, the year would not have been the same without any of you. I'm going to miss all of our random mid-day outings and the jokes we use to make. Special thanks to Khush! You always listened to me complain about everything, I'm going to miss the Sunday night messages in which we stated how we wasted the weekend, but yet we never learnt from our mistake! A huge thanks to my family and friends for the patience and support. I would not have survived the year without all of you.

Lastly, I'd like to thank DAFF for the bursary. A special thanks to Ms Dorah Lekalakala and her team, they definitely went beyond their call of duty to ensure that their students are in a comfortable learning environment.

Plagiarism Declaration

I know that plagiarism is wrong. I have used Harvard convention of citation and referencing. This thesis is my own work.

Signature: Signed by candidate

TABLE OF CONTENTS

List of Figures

Figure 5.10 Vertical sections for three selected dates in box D1 for 2008, for a) Temperature (^{o}C) and density (kg/m^{3}) (white isopycnals) and b) BVF (s^{-2}) and MLD (m) (black line).

Figure 5.11 Vertical sections for three selected dates in box D4 for 2008, for a) Temperature (^{o}C) and density (kg/m^{3}) (white isopycnals) and b) BVF (s^{-2}) and MLD (m) (black line).

List of Tables

Chapter 1

Introduction

1.1 Overview

Primary productivity in the Southern Ocean plays an important role in the mitigation of climate change and the global carbon flux (Schlitzer, 2002; Monteiro et al., 2011). Within the Southern Ocean, the Sub-Antarctic Zone (SAZ) is the region of highest productivity (Thomalla et al., 2011). The dominant mode of variability in the SAZ, characterised by the seasonal cycle of the region (Monteiro et al., 2011), influences the growth of phytoplankton (Boyd, 2002). During winter, the light limitation and deep mixing in the Southern Ocean inhibit phytoplankton growth (Boyd, 2002; Thomalla et al., 2011; Joubert et al., 2014). Increased light and stratification promote the growth of phytoplankton during spring and summer months (Swart et al., 2015).

It is important that we develop an understanding of the physical drivers of the Mixed Layer Depth (MLD) in the Southern Ocean. Physical processes at mesoscale (10 – 100 km), sub-mesoscale (1 – 10 km) and sub-seasonal scales have been shown to influence MLD variability in the Southern Ocean (Lévy et al., 2012). An example of these processes is seen in a study by Thomalla et al. (2011); where the phytoplankton variability during spring and summer was driven by the intra-seasonal changes of the mixed layer (ML) physics. The MLD fluxes are not only controlled by seasonal atmospheric forcing (e.g. winds and heat fluxes) but also by the interaction between the atmosphere and ocean surface boundary layer features (e.g. frontal positions and eddies) (Lévy et al., 2001).

Despite its major role in climate change, logistical restrictions have led to limited data in the Southern Ocean and the understanding of this complex system. The development of global scale Earth System Models (ESMs) allow for better understanding of the dynamics in the Southern Ocean, they are currently producing reliable global annual carbon uptake but have limiting seasonal abilities (Lenton et al., 2013). While in most cases these models are able to capture sea-air carbon dioxide fluxes, they also have difficulty reproducing the exact phase and amplitude of the observed seasonal sea-air carbon dioxide flux (Lenton et al., 2013). A

study by Gruber et al. (2009) has found that these Earth System models produce dependable results on a global scale. To improve these simulations, the horizontal resolution needs to be increased (Lévy, 2008). While most global models with 2^o grid resolution are able to capture large-scale oceanographic features (Gruber et al., 2009), only eddy resolving models are able to simulate improved vertical dynamics (Lévy, 2008). Sub-mesoscale features play a major role in the MLD, if some of these features are not resolved it may result in ±50% error in the primary production estimates (Glover et al., 2008). Increased temporal resolution also allows for improvement in model performance, the models are able to better capture the timing of the spring blooms; however these models still overestimate the peak of the bloom in the Southern Ocean (Mckiver et al., 2014).

These findings hint towards a need to better understand the physical mechanisms of the MLD in the Southern Ocean. This study focuses on the MLD dynamics simulated in the South Atlantic and the Southern Ocean.

This study uses the Regional Ocean Modelling System (ROMS) to run an interannual simulation in the ocean surrounding South Africa. The initial analysis uses an existing ROMS configuration from Loveday (2014), these results are then compared to a second ROMS model configuration which was setup run for 6 years. The modelled domain includes the South West Indian Ocean (SWIO), the South East Atlantic Ocean and the Southern Ocean. The boundary currents in this domain, namely the western boundary Agulhas Current and the eastern boundary Benguela Current are characterised by strong mesoscale (10 -100km) variability giving rise to complex local dynamics.

Swart et al. (2015) highlighted the importance of eddy resolving models in understanding the sensitivity of MLD dynamics. The increase in global model resolution would be expensive in terms of computational power. A possible solution to this is to run a regional model at a $1/4^o$ resolution with an online nested $1/12^o$ resolution child domain located over high variability areas such as the South African boundary currents. This study investigates this possible solution by doing a regional study in the South Atlantic.

This is a comparison study between two model configurations showing how increased horizontal grid resolution over the boundary currents affect MLD in the Sub-Tropical Zone (STZ) and the Sub-Antarctic Zone (SAZ) in the Atlantic sector. Model 1 (Nested Model) is a

two-way nested model with a child domain (1/12^{o}) over the South African boundary currents while the parent domain is simulated at a coarser horizontal scale of 1/4^{o}. Model 2 (Standalone Model) uses the parent configuration only.

1.2 Aim and Key questions of this Project.

The aim of the study is to analyse how increased horizontal grid resolution across areas of strong mesoscale variability, the Agulhas Current and Benguela Current, impact the vertical dynamics in the South Atlantic and the Southern Ocean.

1. Does the increased grid resolution improve the simulation of large scale oceanographic features in the domain?

2. Does the difference in resolution result in any major oceanographic bias?

3. Are these models able to capture MLD seasonality in the STZ and SAZ?

4. How does the improved grid resolution impact the physical drivers of the MLD variability in the STZ and SAZ?

Chapter 2

Literature Review

2.1 The global setting of the modelled domain.

The study area stretches from 26.26°W to 70°E and 49°S to 3.83°N as shown in **Figure 2.1**. As seen in the figure the domain includes the South African coast, the South West Indian Ocean (SWIO), the Sub-Antarctic and a portion of the South Atlantic Ocean.

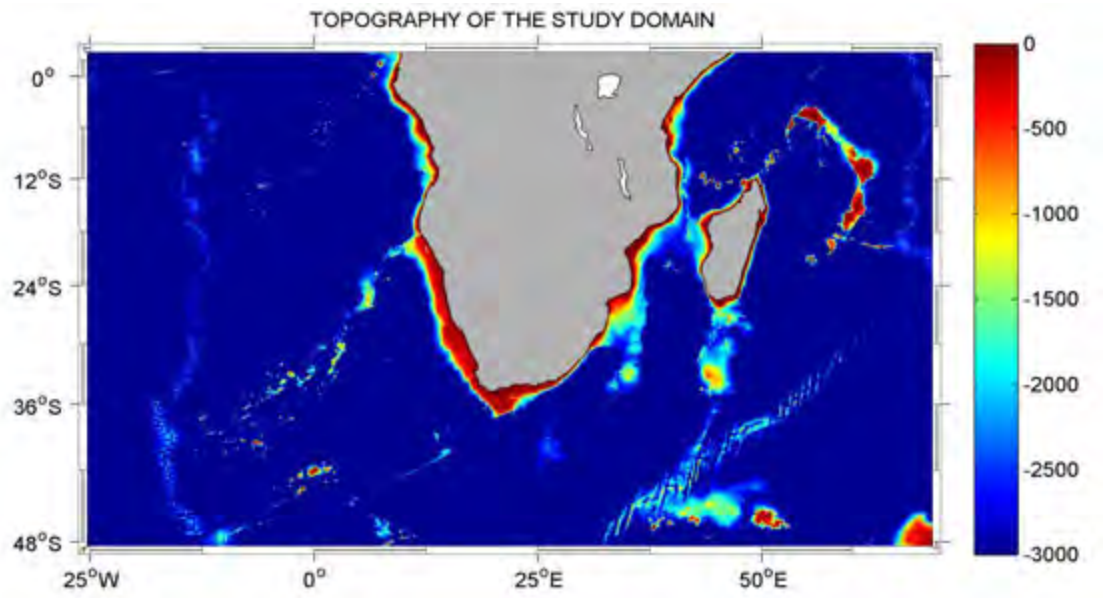

Figure 2.1 Colour map showing the bathymetry of the study domain with a colour bar scale indicating depth of the ocean in meters. The data used is derived from ETOPO2.

2.1.1 The Indian Ocean

The Indian Ocean is the smallest ocean due to its enclosure by the Asian continent in the subtropics (Wyrtki, 1971). The water mass structure is complex in this ocean due to the variable dynamics in this region. Examples of these dynamics include the monsoonal wind regime, the highly dynamical currents and unbalanced precipitation rates between the western and eastern Indian Ocean (Schott et al., 2009; Tomczak and Godfrey, 2013).

In this project, we only focus on the South Western side of the Indian Ocean as it forms part of the modelled domain (**Figure 2.2**). The SWIO is a highly dynamical region with increased seasonal variability (De Ruijter et al., 2005). The region is wind driven and forms part of the anticyclonic subtropical gyre of the Indian Ocean (Stramma and Lutjeharms, 1997). It was suggested that the seasonality in the region is caused by the local wind stress (Stramma and Lutjeharms, 1997).

Tropical and subtropical water masses occupy the upper 500 m of the Indian Ocean (Tomczak and Godfrey, 2013). The Intermediate layer of the SWIO is mainly occupied by Antarctic Intermediate Water (AAIW) (Beal et al., 2006), whilst the deep layer (>1500 m) of the SWIO is occupied by Indian Ocean Deep Water (Tomczak and Godfrey, 2013).

The large scale flow regime of the SWIO region of the modelled domain is dominated by five oceanographic features present in this region. The major westward-flowing South Equatorial Current (SEC) flows south of 10^{o}S until it reaches the island of Madagascan. At this point, the SEC splits in two. The resulting northward flow forms the North-East Madagascan Current (NEMC), which continues to flow westward where it splits and forms the southward flowing Mozambique Channel eddies, which is in the form of anticyclonic mesoscale eddies (De Ruijter, 2005). The southward portion of the SEC forms the South-East Madagascan Current (SEMC), a southward-flowing western boundary current like flow (Lutjeharms, 2006). The Mozambique Channel eddies along with the SEMC forms the northern extension of the Agulhas System. The poleward flowing AC is the western boundary current hugging the South African coast (Lutjeharms, 2006). The Agulhas Current transports tropical water (temperature >22^{o}C) southward at a speed of >2 m/s (Lutjeharms, 2006). The southern portion of the current has increased meandering due to the shear, which develops at the wide continental shelf of the Agulhas Bank (De Ruijter et al., 1999). The current overshoots the African continent where it enters the South Atlantic, the current then turns on itself forming the Agulhas retroflection (Gordon et al., 1987). This leads to the formation of the Agulhas Return Current (ARC), an eastward flowing current which meanders between 35^{o}S and 45^{o}S (Lutjeharms, 2006).

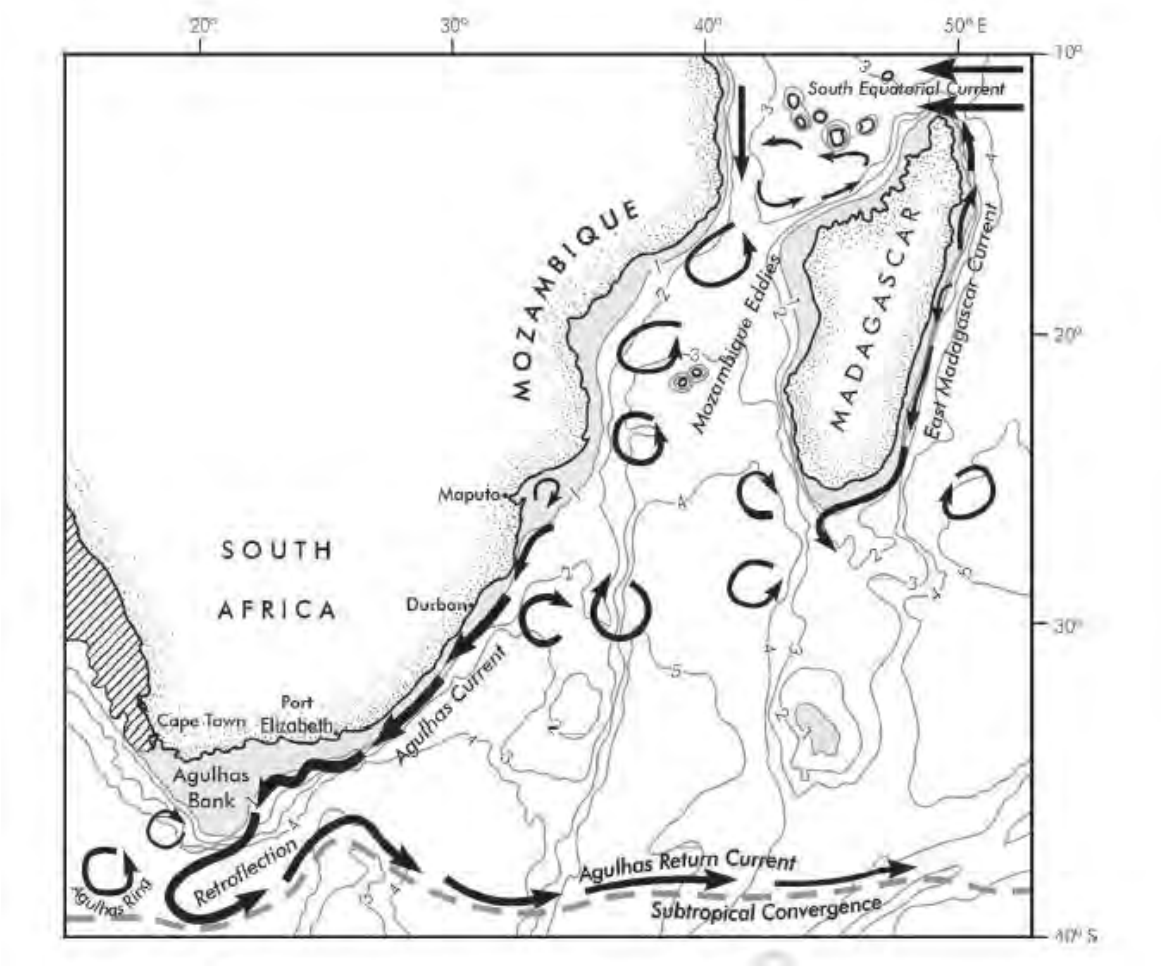

Figure 2.2 The ideal flow regime in the greater Agulhas system in the SWIO, the contours shows the bathymetry of the region (km) whilst arrows indicate direction of flow. (Adapted from Lutjeharms, 2006)

2.1.2 <u>The Southern Ocean</u>

The Southern Ocean forms a major part of the global climate system. It plays an important role in the global carbon cycle due to its unique circulation which allows for the exchange of natural gases between the ocean and the atmosphere (Moigne et al., 2012). It is the formation site of AAIW, Sub-Antarctic Mode Water (SAMW), and Antarctic Bottom Water (AABW) (Moigne et al., 2012). These water masses help with the transport and distribution of anthropogenic carbon dioxide (CO_2) across the global oceans (Caldeira and Duffy, 2000; Moigne et al., 2012). The region is characterised by the pronounced meridional gradient in the surface temperature and salinity (Deacon, 1933). The northern part of the Southern

Ocean meets with the warm and salty subtropical water whilst the southern extent consists of cold Antarctic water (Trenberth et al., 1990). The region is dominated by a circumpolar eastward flowing current, the Antarctic Circumpolar Current (ACC) (Nowlin et al., 1977; Trenberth et al., 1990); it is the most intense eastward flowing current and is driven by the westerly winds in the region. The current appears between 45^{o}S and 55^{o}S and connects the global ocean basins (Trenberth et al., 1990; Orsi et al., 1995) due to its unrestricted circumpolar flow.

2.1.2.1 The Sub-Tropical and Sub-Antarctic Fronts in the South Atlantic Sector

The north to south gradients in the Southern Ocean can be characterised by frontal bands defined by Orsi et al. (1995). The positions of these frontal bands are not identical in all sectors of the Southern Ocean (Sokolov and Rintoul, 2002; Billaney et al., 2010). The frontal bands, shown in **Figure 2.3**, can be located using a subsurface temperature criteria described by Orsi et al (1995). Swart et al (2008) was able to locate the positions of these fronts using altimetry data, thus making it easier to locate the frontal bands using satellite data.

The northern extent of Sub-Antarctic Surface Water (SASW) meets with the Sub-tropical Surface Water thus generating a large property gradient. The large gradient indicates the position of the Sub-Tropical Front (STF), which is located by finding the northward increase from 10 to 12^{o}C at 100 m (Orsi et al., 1995). The surface water north of the STF is warmer than 11.5^{o}C and saltier than 34.9 psu (Deacon 1933), water south of the STF is colder and fresher than that of the water north of the STF.

The transition from Sub-Antarctic to Antarctic water occurs south of the Sub-Antarctic Front (SAF) (Whitworth and Nowlin, 1987). At the SAF, the AAIW is deeper than 500 m and is defined by a subsurface temperature minimum (Whitworth and Nowlin, 1987; Orsi et al., 1995). The area between the SAF and Antarctic Polar Front (APF) is known as the core of the ACC, Orsi et al. (1995) located the SAF by finding the subsurface temperature >4-6^{o}C at 400 m. Another method was presented by Park et al. (1993); they found the SAF by locating the 6^{o}C isotherm at 200 m.

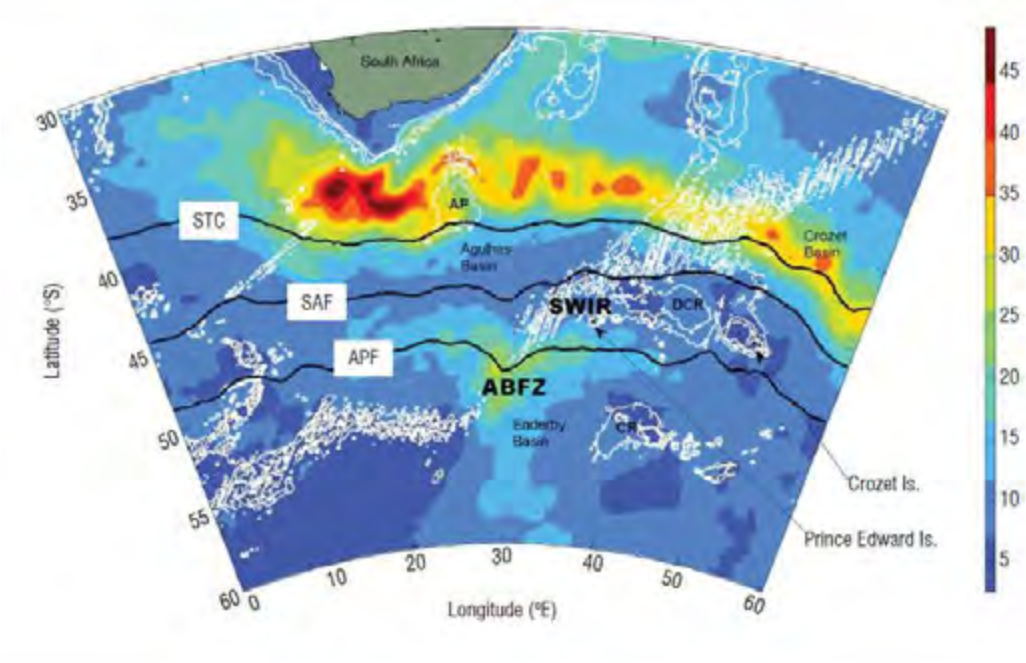

Figure 2.3 The annual mean positions of the fronts, namely the STF (denoted as STC) and the SAF south of Africa. The figure also shows the mean position of the Antarctic Polar Front (APF) The colour shows the bathymetry (m). The figure also includes the position of the South West Indian Ridge (SWIR) and the Andrew Basin Fracture Zone (ABFZ). (Adapted and Modified from Durgadoo et al., 2010)

2.1.3 The South Atlantic Ocean

The South Atlantic climate is dominated by the presence of the semi-permanent subtropical high-pressure system (Höflich, 1984).

The South Atlantic is seen as the link between the North Atlantic and the rest of the global oceans (Rintoul, 1991). Roemmich (1983) showed that ±10 Sv of the South Atlantic surface water is transported northward; this northward transport is compensated by the southward transport of North Atlantic Deep Water (NADW). The circulation in the South Atlantic is dominated by the wind driven anticyclonic subtropical gyre (Peterson and Stramma, 1991).

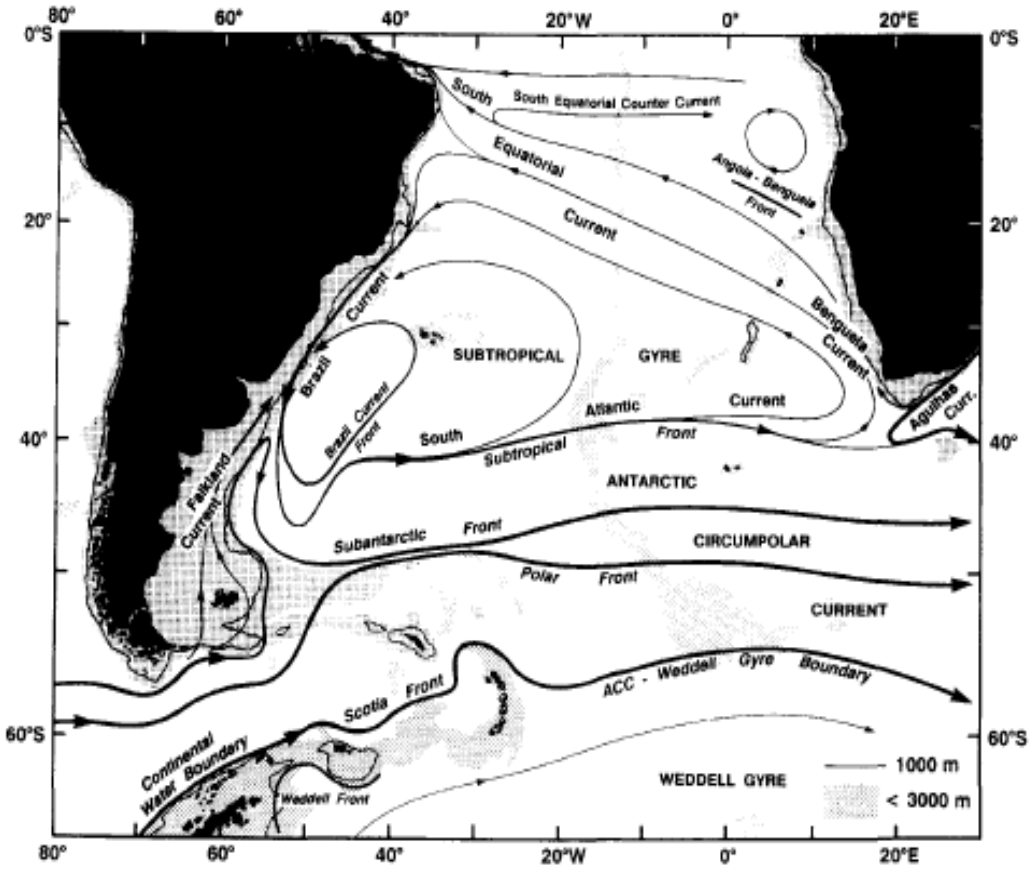

Figure 2.4 The general flow regime in the South Atlantic along with fronts and major currents in the regions. (Adapted from Peterson and Stramma 1991).

The study domain is mainly focused on the currents and features on the eastern side of the South Atlantic. A small amount of Indian Ocean water is leaked into the South Atlantic; this intermittent leakage occurs as rings formed at the Agulhas retroflection flows into the South Atlantic (Lutjerharms and Gordon, 1987). These rings transport salt and heat into the South Atlantic (Lutjerharms and Van Ballegooyen, 1988). This transport is enhanced by the presence of Agulhas filaments, which in turn enhances the westward transport of Indian Ocean water. The dominant current in this section of the study domain is the Benguela Current. This is the eastern boundary current of the South Atlantic sub-tropical gyre (Veronis, 1973); it is a broad northward-flowing current along the west coast of South Africa (Peterson and Stramma, 1991). The Benguela Current has three origins namely; central Atlantic water, Indian Ocean water (from Agulhas leakage) and a blend of tropical Atlantic

and Agulhas water (Garzoli and Gordon, 1996). The current forms an important part of the South Atlantic Meridional Overturning Circulation (MOC) (Garzoli and Gordon, 1996). The northward geostrophic transport of the Benguela Current is ±18 Sv at 30^{o}S (Stramma and Peterson, 1990). The thermohaline fluxes of the northward flowing currents help balance the Southward meridional flux by somewhat balancing the poleward flow of the Brazil Current

2.2 Zones of interest in the South Atlantic.

This project focuses on the Mixed Layer Depth (MLD) in the Sub-Tropical Zone (STZ) and the Sub-Antarctic Zone (SAZ). This section gives a brief overview of the positions of these zones.

The transition from the tropical to sub-tropical regime forms the STZ. The Angola-Benguela front marks the northern extent of the STZ in the Southeast Atlantic reaching 18^{o}S in some areas (Meeuwis and Lutjeharms, 1990). The southern limit of the STZ is marked by the STF (Mercier et al., 2003) (**Figure 2.3**).

The SAZ is the transitional zone between the colder Antarctic water and the warmer and saltier subtropical surface water. The SAZ is positioned between the STF and the SAF (**Figure 2.3**). Swart and Speich (2010) described the latitudinal range of SAZ to be between 38.2 and 46.8^{o}S and a mean width of 540 km along the GoodHope line. The position of the SAZ is highly variable; this variability is controlled by the heat and salt influx due to the presence of Agulhas Rings (Swart and Speich, 2010).

2.3 Problem Identification

The upper layer of the ocean is vertically isothermal with a uniform density which exists due to vigorous turbulent mixing (de Boyer Montégut et al., 2004). The extent of this layer, known as the Mixed Layer Depth (MLD) is controlled by kinetic energy, potential energy, heat fluxes and freshwater fluxes (Thomson and Fine, 2003; Jackson et al., 2010). This mixed layer allows for interaction between the upper ocean and the atmosphere (Lalli and Parsons, 1995); it plays an important role in ocean ventilation, water mass formation (Iwasaka et al., 2006) and the evolution of sea surface temperature (SST) (Chu and Fan,

2011). The mixed layer also plays an important role in the global ocean and climate as it is the layer of high productivity (Chu and Fan, 2011).

The MLD is defined as the depth at which the temperature difference exceeds 0.2^{o}C below a reference depth of 10 m (de Boyer Montégut et al., 2004). The highest variability of the MLD is seen in the Southern Ocean and the North Atlantic, whilst minimum variability is seen in the tropics (Carton et al., 2008). The MLD is deepest in winter whilst spring restratification initiates shoaling of the MLD (Juza et al., 2012).

Most of the data used to study the MLD comes from ship-based observations, these datasets are spatially and temporally limited (Otobe et al., 2003), with some exceptions of longer term studies in particular areas (e.g. Cronin and Kessler, 2002; Jackson et al., 2010). Limited temperature and salinity data are available in most of the global oceans; these datasets are however slowly growing due to the contribution of the International Argo Project which started in 2000 (The Argo Science Team, 2000), which will directly increase the MLD data. Very few studies have produced a global MLD climatology (de Boyer Montégut et al., 2004) and as a result, there is a need for more data.

The limited data has led to the development of numerical ocean models, which have improved in recent years due to the increase of computational power available (Mckiver et al., 2014). Models are generally able to capture MLD seasonality (Kara et al., 2000), with slight variations seen in the restratification onset. In recent years' models have been able to achieve greater resolution by better computing large-scale dynamics and assimilating the external forcing (Griffies et al., 2005). Many global models are able to capture large scale processes whilst still containing some regional scale bias (Vichi and Masina, 2009; Mckiver et al., 2014). The resolution of these models play a major role in the distribution of the bias, in many studies, the biogeochemistry of the models is compromised due to the sensitivity to minor changes in physical processes (Mckiver et al., 2014).

The resolution of global models, as well as their numerical schemes, needs to be improved to better simulate the deep ocean, its boundaries and the interaction between the ocean and the atmosphere (Penduff et al., 2007; Lévy, 2008). The DRAKKAR consortium coordinates the development of high resolution global ocean models, allowing for better understanding of the variability in the ocean and atmosphere (Penduff et al., 2007). These

future ocean and climate predictive models will be simulated at a resolution which is eddy permitting and eddy resolving, i.e a resolution >1/4^{o} on a horizontal scale.

Models with a grid resolution capable of resolving mesoscale and sub-mesoscale features have been shown to have stronger vertical mixing (Lévy, 2008). Mckiver et al. (2014) have shown that low resolution models are unable to correctly simulate the vertical dynamics; which leads to model bias. The higher resolution global models (>1/4^{o}) capture a deeper MLD and faster restratification than that of the low resolution (2^{o}) model (Mckiver et al., 2014). Mckiver et al. (2014) did a comparison study using a high resolution (1/4^{o}) and a low resolution (2^{o}) PELAGOS (Vichi et al., 2007) model, they found the sea surface salinity and the SST are comparable for the two models, with bigger differences seen in the MLD. The DRAKKAR group model (1/4^{o} model resolution) showed an MLD twice that of the observed MLD, with no temperature bias in that area (Juza et al., 2012). During summer months, global models underestimate MLD whilst overestimating the MLD during winter months (Juza et al., 2012), this is an effect of the physical processes which impact the MLD (Lévy et al., 2012). This suggests that the global models misrepresent seasonal cycles associated with the various physical processes which influence the MLD. It could be a result of increased mesoscale and sub-mesoscale variability which stimulates vertical transport (Lévy et al., 2008) or increased stratification due to solar heating. Simulated MLD is generally overestimated by 10 to 30% during winter; this overestimation can be corrected by the calibration of the atmospheric forcing of model physics (Juza et al., 2012).

The data in the Southern Ocean is especially limited due to logistical restraints. In a study by Garabato et al. (2004), it is shown that the Southern Ocean undergoes intense local mixing events. Due to limited data these events are not always well captured. Mesoscale and sub-mesoscale variability drive spring restratification in the SAZ whilst the increased summer radiation continues to increase the stratification in the water column (Swart et al., 2015). The climatology data from de Boyer Montégut et al. (2004) indicates SAZ experiences the maximum MLD from June to October. Models are used to simulate the ocean conditions to get a clear understanding of the dynamics leading up to the intense mixing events.

Earth System Models (ESMs) are used to study Southern Ocean dynamics and are currently producing reliable global annual carbon uptake but have limiting seasonal abilities (Lenton

et al., 2013). Gruber et al., 2009 has also found that these ESMs produce dependable results on a global scale. The Nested Model Intercomparison Model Project phase 5 (CMIP5) was used to focus on the Southern Ocean in a study by Meijers (2014). In this ESM, it is shown that with greater resolution (still too coarse to permit mesoscale features) and improved numerical schemes the simulated MLD was an improvement to the MLD simulated in CMIP3. The MLD in CMIP5 was found to be shallower than observed MLD, which is likely to be a result of salinity concentration rather than of the temperature of the water column (Meijers, 2014).

Chapter 3

Data Methodology

This thesis uses the Regional Ocean Modelling System (ROMS) to resolve large scale features around the Southern African continent (**Figure 2.1**). The study uses a ROMS configuration set up by Loveday (2014). Loveday (2014) used the ROMS model's nesting ability to achieve higher resolution over the South African boundary currents by using an online AGRIF nested 1/4^{o} and 1/12^{o} configuration. This model configuration is referred to as the nested model. This chapter describes the model configuration for both the parent and child domain. This study removed the nested child domain and ran the coarser parent domain configuration, referred to as the standalone model. This allows for a comparison study on the impact fine scale resolution on the vertical dynamics in the STZ and SAZ in the Atlantic sector.

3.1 Model Description

ROMS is a three dimensional free surface terrain following (sigma coordinate) model which computes the orthogonal physical properties in the Arakawa C-grid on an earth rotating frame. It uses split-explicit time stepping to solve the hydrostatic primitive equations using higher order numerical schemes (Shchepetkin and McWilliams, 2005). ROMS uses the hydrostatic and the Boussinesq approximations to solve the Reynolds-averaged Navier-Stokes equations (Shchepetkin and McWilliams, 2005).

The basic equations are shown below:

$$\frac{\partial u}{\partial t} + v.\nabla u\text{-f}v = -\frac{\partial P}{\partial x} + \mathrm{F}_u + D_u \quad (1)$$

$$\frac{\partial v}{\partial t} + u.\nabla v + \text{f}u = -\frac{\partial P}{\partial y} + \mathrm{F}_v + D_v \quad (2)$$

$$\frac{\partial P}{\partial z} = -\frac{\rho g}{\rho_0} \quad (3)$$

$$\frac{\partial u}{\partial x} + \frac{\partial v}{\partial y} + \frac{\partial w}{\partial z} = 0 \quad (4)$$

$$\frac{\partial T}{\partial t} + v\nabla T = \mathrm{F}_\mathrm{T} + D_\mathrm{T} \quad (5)$$

$$\frac{\partial S}{\partial t} + v\nabla S = \mathrm{F}_\mathrm{S} + D_\mathrm{S} \quad (6)$$

Equation (1) and (2) represents the horizontal momentum. Equation (3) represents the hydrostatic balance and the mass balance is shown by equation (4), continuity equation. Equation 5 and 6 are the conservation equations for temperature (T) and the salinity (S).

In these equations

- x,y,z are the zonal, meridional and vertical directions (m) on a Cartesian plane system.
- u, v, w are the vector velocity (m/s) components in the x,y,z directions.
- t is time in seconds (s)
- f is the coriolis parameter (s^{-1})
- T is potential temperature (°C)
- S is salinity
- P is the dynamic pressure (m^2/s^2)
- F_u, F_v, F_T, F_S are terms for possible forcing

- D_u, D_v, D_T, D_S are the dissipative terms

- ρ the density of seawater (kg/m^3), and ρ_0 is the reference density of seawater (1025kg/m^3)

- g is the acceleration of gravity (m/s^2)

3.2 The Nested Model Configuration

The parent configuration, SAFR-4, resolves large scale features in the oceans around Southern Africa (Loveday, 2014). The domain stretches from 26.25°W to 70°E and 49°S to 3.83°N (**Figure 2.1**). The SAFR-4 model configuration was created at 1/4° grid resolution, with 42 vertical layers concentrated at the surface where the vertical s-coordinate surface stretching(θ_s) $= 6$, vertical s-coordinate bottom stretching (θ_b) $= 0$, vertical s-coordinate parameter of transition between depths (hc) =10 and the s-coordinate transformation (vtransform) =1. The nested child domain stretches from 4.33°E to 34.42°E and 45.56°S to 16.99°S. The child domain is 1/12° grid resolution, SAFR-12 (Loveday, 2014).

The two configurations, parent and child, are connected via a two way AGRIF routine. The SAFR-AGRIF grids were created using the standard ROMSTOOLS (Penven et al., 2008). The SAFR-AGRIF uses the GLS (K-KL) scheme to parameterise turbulent mixing in the domain. This mixing scheme, described in Warner et al. (2005), is a two equation model which uses the relationship between the equations to calculate transport and turbulence in the water column.

The surface fluxes of the model are forced with 6 hourly Climate Forecast System Reanalysis (CFSR) fields (Saha et al., 2010). The open boundaries of the domain are forced with the monthly hindcast from Simple Ocean Data Assimilation (SODA) v.2.2.4 (Carton and Giese, 2008). The topography in SAFR-AGRIF is derived from the ETOPO2 dataset (U.S. department of Commerce, National Geophysical Data Centre, 2006). The SAFR-4 topography is smoothed such that the r=grad(h)/h is less than 0.25. The topography of the child domain is smoothed using ROMSTOOLS (Penven et al., 2008) to avoid numerical instabilities caused by sharp horizontal pressure gradients at the interface between the two models (Loveday, 2014). The simulation has a spin up period of ten years (repeats 1979) after which the model run from 1979 to 2010.

3.3 The Standalone Model Configuration

Due to time and computational limitations the simulation of the standalone model only runs from 2005 to 2010. This model configuration uses ROMSTOOLS to remove the child grid from the SAFR-AGRIF configuration. The new configurations, SAFR-4.2, uses the SAFR-AGRIF 2004 outputs to restart the simulation. The standalone simulation then runs from 2005 to 2010, it has a grid resolution of 1/4^{o} throughout the domain (Parent configuration). Computations for the standalone model were performed using facilities provided by the University of Cape Town's ICTS High Performance Computing team: http://hpc.uct.ac.za.

3.4 Description of Data used in model simulation and model validation

3.4.1 New CNES-CLS09 Mean Dynamic Topography (MDT)

The new global MDT, with resolution of 1/4^{o} x 1/4^{o} , is computed for a time period 1993-1999, by using five years of Gravity Recovery and Climate Experiment Data (GRACE) and in situ dynamic height ranging from 1993-2008. The details of the dataset can be found in Rio et al. (2011).

3.4.2 Pathfinder Sea Surface Temperature (SST)

SST data derived from an Advanced Very High Resolution Radiometers (AVHRR) product. Pathfinder SST has a 9 km resolution (Casey and Cornillon, 1999).

3.4.3 Temperature and Salinity Climatology from World Ocean Atlas 2009 (WOA09)

The World Ocean Atlas monthly climatology dataset has a 1°×1° grid resolution (Conkright et al., 2002). The WOA09 variables used in this study are temperature climatology and the salinity climatology (Antonov et al., 2010).

3.4.4 Observed MLD

The observed and modelled MLD is determined using the 0.2^{o}C temperature criterion described in de Boyer Montégut et al. (2004). Two data sets are used:

a) Argo profiling float MLD. The climatology is constructed from 10 day profiles collected between 2005 and 2009 for this study. The data is 1^{o} x 1^{o} regular gridded data (Hasoda et al., 2010).
b) A 2^{o} resolution global MLD climatology (de Boyer Montégut et al., 2004).

3.5 Criteria used to define the Sub-Tropical Front (STF) and Sub-Antarctic Front (SAF)

The positions of the fronts are identified using subsurface temperature criteria (Orsi et al., 1995). The position of the Sub-Tropical Front (STF), is located by finding the northward increase from 10 to 12^{o}C at 100 m (Orsi et al., 1995). The SAF is located using a criteria described in Park et al. (1993); the SAF position is located by finding subsurface 6^{o}C isotherm at 200 m.

Chapter 4

Observation and Model Data Comparison

The key question for this chapter is whether or not the nested and standalone model was able to correctly simulate large scale mean states in the modelled domain.

This chapter focuses on the ability of each of the models to correctly, and satisfactorily simulate the mean state of the ocean in the modelled domain. Each of the models has been simulated for the same domain. The nested model is a two-way nested model with a child domain of increased grid resolution over the South African boundary currents. The standalone model has been run for the same domain but without the child domain. Since the main aim of this project focuses on the MLD dynamics, this chapter analyses the mean state of variables which influence the MLD. The variables analysed are geostrophic flow, Agulhas leakage, Sea Surface Temperature (SST), Sea Surface Salinity and water masses.

4.1 Mean Sea Surface Geostrophic Flow field

SSH streamlines are used to represent the geostrophic flow field in the domain, where the direction of flow is shown using arrow heads. The large scale features and currents analysed are SEC, NEMC, SEMC, Mozambique Eddies, Agulhas Currents, Agulhas Retroflection, ARC, the Benguela Current and the ACC. **Figure 4.1** shows the difference between the two models mean dynamic topography. This figure suggests that the main differences between the models occur in the southern part of the domain and is more pronounced in the Agulhas Current and Retroflection regions. Observational absolute mean dynamic topography, a new CLS-CNES09 product (Rio et al., 2011, **Figure 4.2a**)**,** is compared against model derived streamlines**. Figure 4.2b** and **Figure 4.2c** shows nested and standalone modelled SSH, respectively. The model flow fields are derived from six-year climatology. Each of the figures shows the geostrophic flow using contours with 7cm spacing.

Comparing both of the models geostrophic flow fields to the observed flow field will help evaluate the performance of each of the models. This section focuses on the large scale flow in the region.

Table 4.1 shows the performance of each model compared to the observed data, **Figure 4.2a**. Large scale flow of each model is rated according to the closeness and meandering of each of the features as compared to **Figure 4.2a.** In the case where the model matches the flow of the observed data the key word "present" is used in the table.

Table 4.2 Summary of model performance compared to RIO 2009 data.

Large Scale Flow	**Nested Model (Figure 4.2b).**	**Standalone Model (Figure 4.2c).**
SEC	More intense flow.	More intense flow.
NEMC	Present.	Present.
SEMC	Present.	Present.
Mozambique Channel Flow	Present.	Present.
AC	Weaker flow.	Wider and weaker flow.
Agulhas Retroflection	Present, slightly weaker flow.	No clearly defined path.
ARC	Weaker and more meandering.	Weaker.
Benguela Current	Current intensity and meandering increased.	Current intensity increased.
ACC	Increased meandering.	Increased meandering.

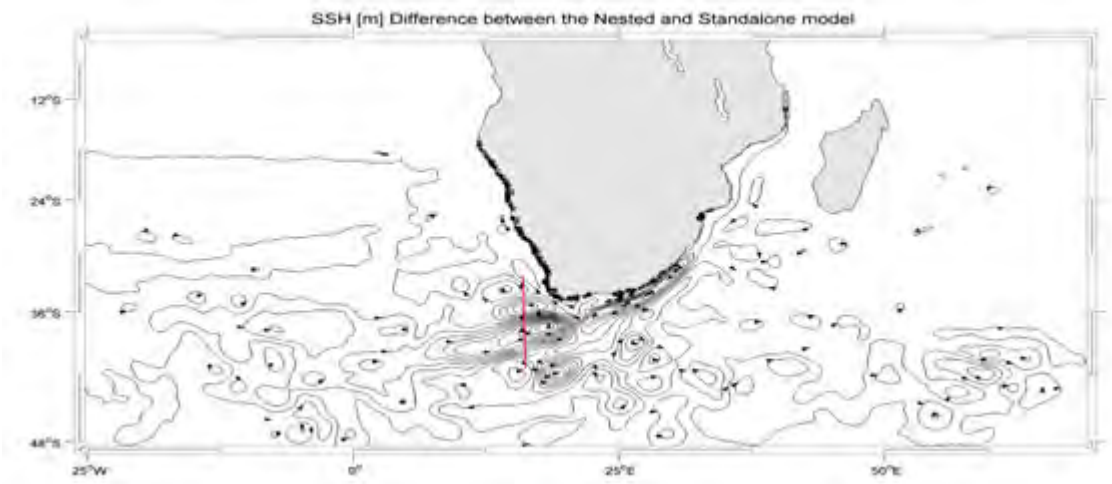

Figure 4.1 Annual mean Sea surface height (SSH) difference between the models. SSH is shown using 7cm contour line spacing with arrows showing direction of derived geostrophic flow.

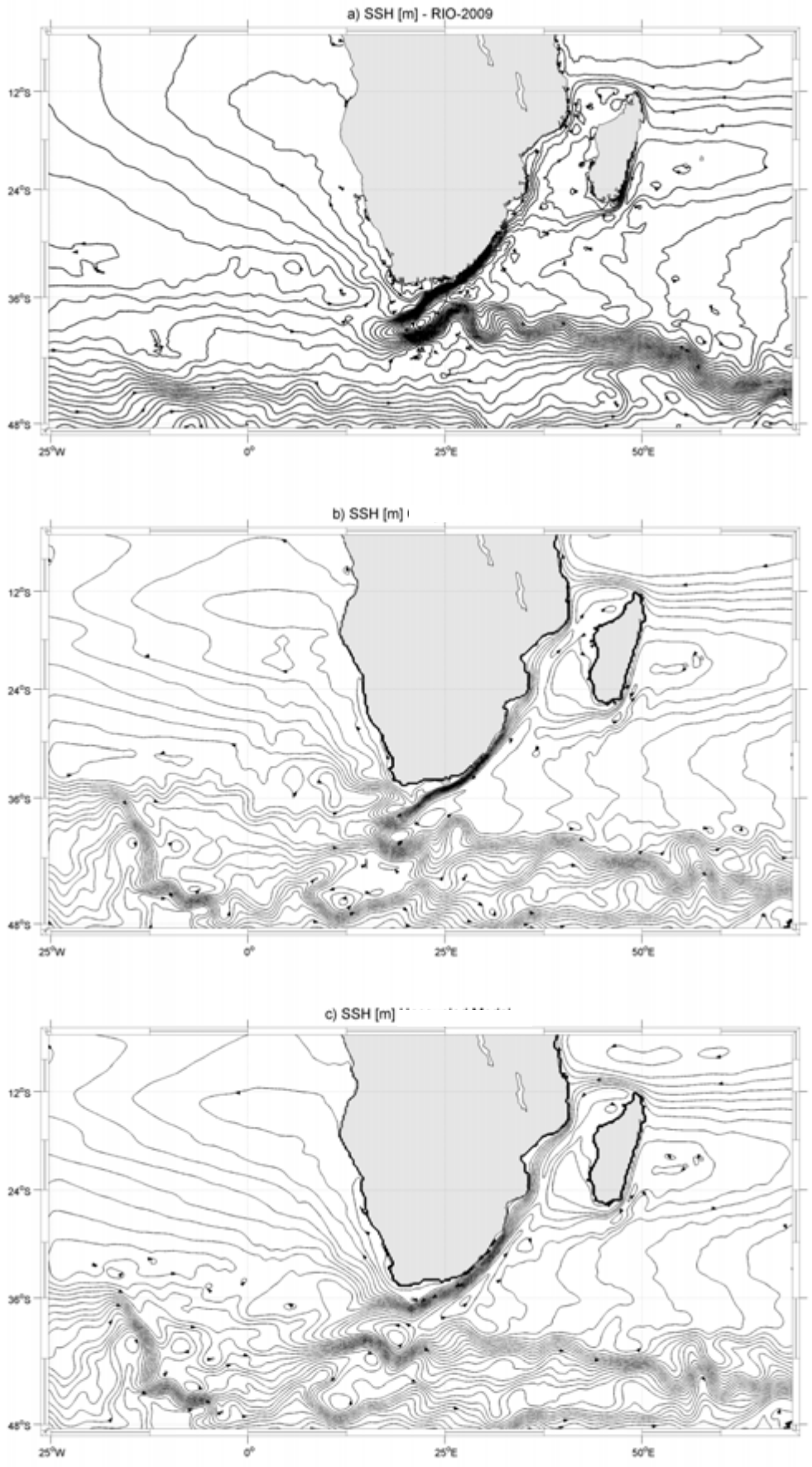

Figure 4.2 Annual mean Sea surface height (SSH) for a) The new CNES-CLS09 data, b) Nested model and c) Standalone model. SSH is shown using 7cm contour line spacing with arrows showing direction of derived geostrophic flow.

4.2 Mean Volume Transport across a line at 17°E between 32° and 43° S

The negative transport across this line represents the volume of water from the Indian Ocean which is leaked into the South Atlantic Ocean (Agulhas leakage). **Figure 4.3** is a time series for the upper 1500m of the water column for both models. Line shown in **Figure 4.1**, red line.

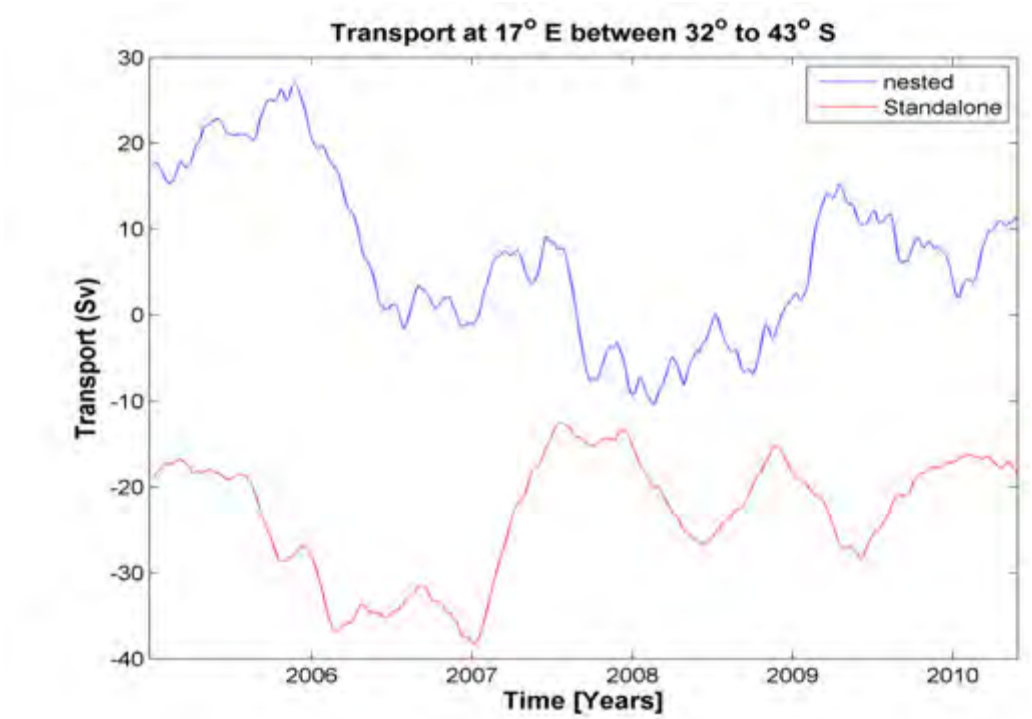

Figure 4.3 Time-series of (moving mean) transport across upper 1500 m for line at 17° E

Both models show evidence of a seasonal signal for transport across this line, with increased westward transport during winter. The Nested model shows higher eastward transport compared to the standalone model. The annual mean transport across the line for the nested model and the standalone model is -13.77 and -23.18 Sv, respectively. Gordon et al. (1992), found Agulhas leakage to be -15 Sv, thus the nested model has a leakage value closer to the leakage shown in literature. The standalone model has a leakage of 8.13 Sv more than Gordon et al. (1992).

4.3 Sea Surface Temperature and Salinity

The surface properties of the ocean contribute to the dynamics of the water column. This section looks at the surface temperature and salinity of each model and observed data. The purpose of this section is to find whether or not either of the models correctly simulated these surface conditions.

The first variable investigated is the mean SST of the region. Pathfinder SST data is used for comparison to each of the models. The SST in the north east section of the domain is overestimated by 2^0C in both models. The small warm plume off the North West coast of Madagascar, observed in **Figure 4.4a**, is larger in both models. The higher temperature Indian Ocean water in the Agulhas current extends more westward in the models, where the standalone model, **Figure 4.4c**, has a more surface area covered by Indian Ocean water present in the Atlantic Ocean. In the Atlantic sector of the domain, the models simulate the increasing isotherms moving northward, as seen in the observed data. In the observed data, a small plume of higher temperature is observed in the North West section of the domain. The small plume is exaggerated in both models with the higher isotherm extending from the western boundary of the domain to the west coast of Africa.

To further analyse the ability of the models to simulate the SST in the domain, the mean difference of SST is analysed (nested SST minus standalone SST, **Figure 4.5a**). The mean difference shows the standalone model having the higher temperature in the Indian Ocean SAZ.

Four boxes, 2^0x2^0, are randomly chosen to further investigate seasonal trends of the SST in the domain. Boxes A1 and B1 lie within the STZ, whilst C1 and D1 lie within the SAZ.

The seasonal cycle constructed for each of the boxes are shown in **Figure 4.5b.** The modelled SST in the boxes is compared to Pathfinder SST data to analyse the performance of the models in the various regions. The models correctly simulate the seasonality found in the Pathfinder data. The SST in the SAZ is lower than that of the SST in the STZ. In the STZ box A1 shows both models overestimating SST by ±1^{o}C during summer and spring. Box B1 shows both models underestimating SST during summer. In box B1 the standalone model

overestimates SST during winter by ±1^{o}C whilst the nested model simulates winter SST <0.1^{o}C higher than that of the pathfinder SST data.

The models largely correctly simulate the SST during summer in box C1. The models do, however, underestimate the SST by ±5^{o}C during winter. Box D1 in the SAZ shows both the nested and standalone model overestimating SST. The nested model overestimates SST by ±2^{o}C whilst the standalone model overestimates the SST by ±4^{o}C. The overestimation of temperature in the SAZ a result of boundary conditions which is overestimating the temperature or that there may be an imbalance in the surface heat fluxes over the open ocean.

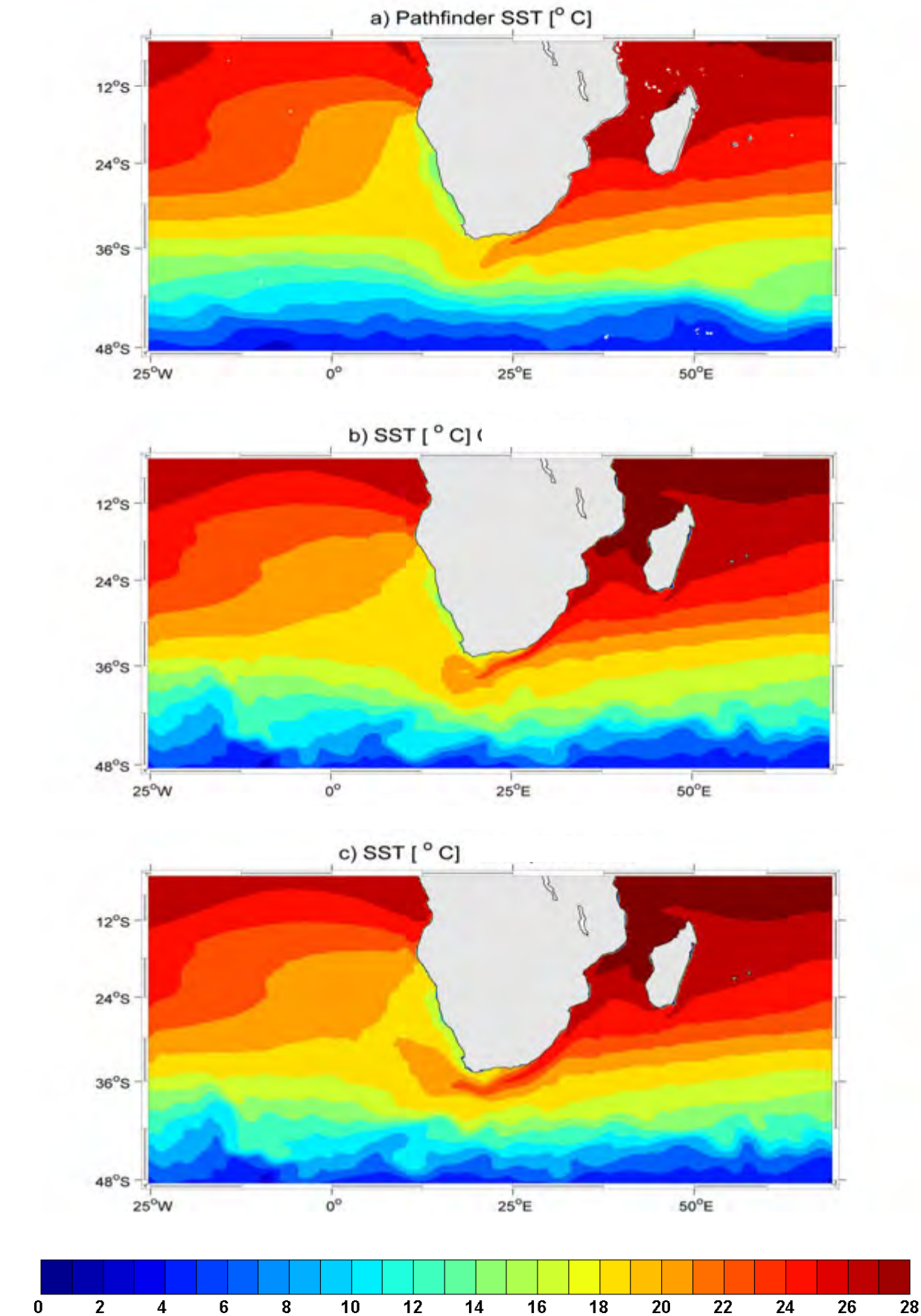

Figure 4.4 Mean Sea Surface temperatures (°C) of the domain for a) Pathfinder, b) Nested model and c) Standalone model data.

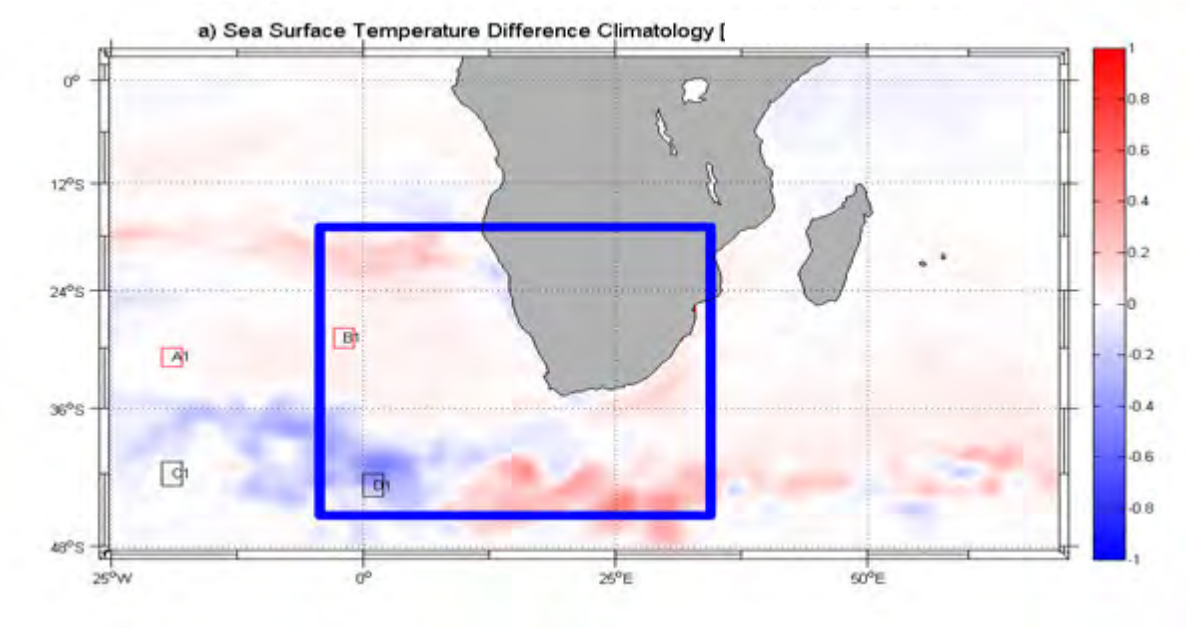

b)

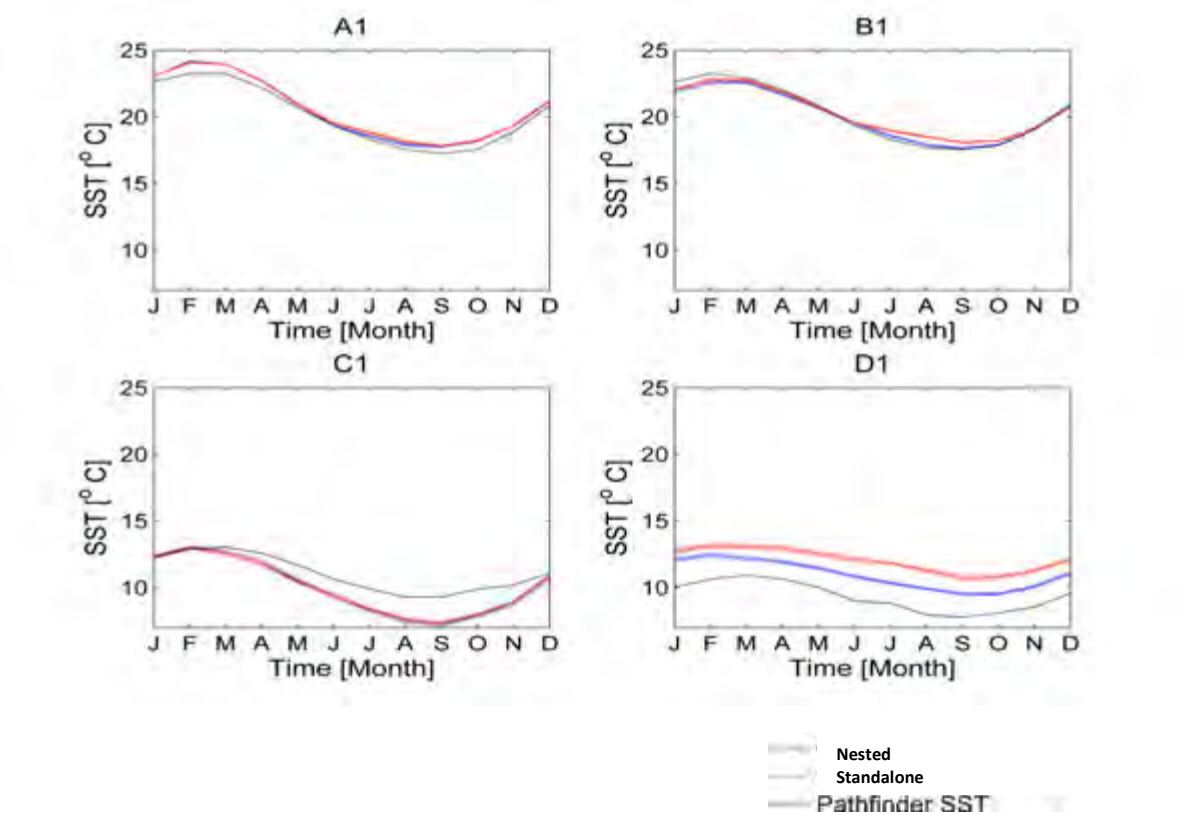

Figure 4.5 Mean Sea Surface Temperature (^{O} C) a) Difference between the nested and standalone model Blue box shows region where the nested model child nest is located and smaller boxes represent regions chosen for further investigation and b) Time-series for the four boxes of a monthly climatology.

The next variable analysed is the mean Sea Surface Salinity. WOA09 (Antonov et al., 2010) mean Sea Surface Salinity is used to analyse each models ability to simulate surface salinity in the domain. The northeast section of the domain has a low salinity tongue (**Figure 4.6a**); this fresh salinity tongue is present in the nested and standalone models, **Figure 4.6b** and **c**. The WOA09 data (**Figure 4.6a**) shows the fresh salinity tongue with a salinity of 34.75 psu, characteristic of Indian Ocean Tropical Surface Water. The models, however, contain a fresher salinity tongue with a salinity as low as 34.25 psu. The models also show a salinity tongue extending further westward.

All the datasets show the presence of a high salinity tongue present in the south-east section of the domain. This tongue contains water with a salinity of 35.5 psu, characteristic of Indian Ocean Subtropical Surface Water (Lutjeharms, 2006). The observed climatology data (**Figure 4.6a**) show a westward extension to 30^{o}E whereas the high salinity tongue only extends to 65^{o}E in each of the models.

Figure 4.6 shows the models having a correctly simulated salinity in the region around the South African coast, where the salinity is ±35.25 psu. The models also correctly simulate low salinity water in the southern part of the domain. The higher salinity isolines of both the nested and standalone model (**Figure 4.6b and c**) protrude further southward than that of the WOA09 (**Figure 4.6a**) isolines in the southern part of the domain.

The north-west side of the domain shows the observed data having (**Figure 4.6a**) high salinity water extending further south than that of the models. The 36.5 psu isoline extends to 28^{o}S in the observed surface salinity, whereas it isoline only extends to 24^{o}S in the nested and standalone model (**Figure 4.6b** and **c)**. This does, however, have a further eastward extension in the model simulated surface salinity.

Further analyses are performed on the difference between the two models. This is done by finding the mean difference between the two models, nested and standalone, surface salinity (**Figure 4.7a**). The nested model has higher salinity concentrations in the ARC, Agulhas Current as well as the STZ. The negative values in the figure also indicate the increased salt input into the SAZ in the standalone model.

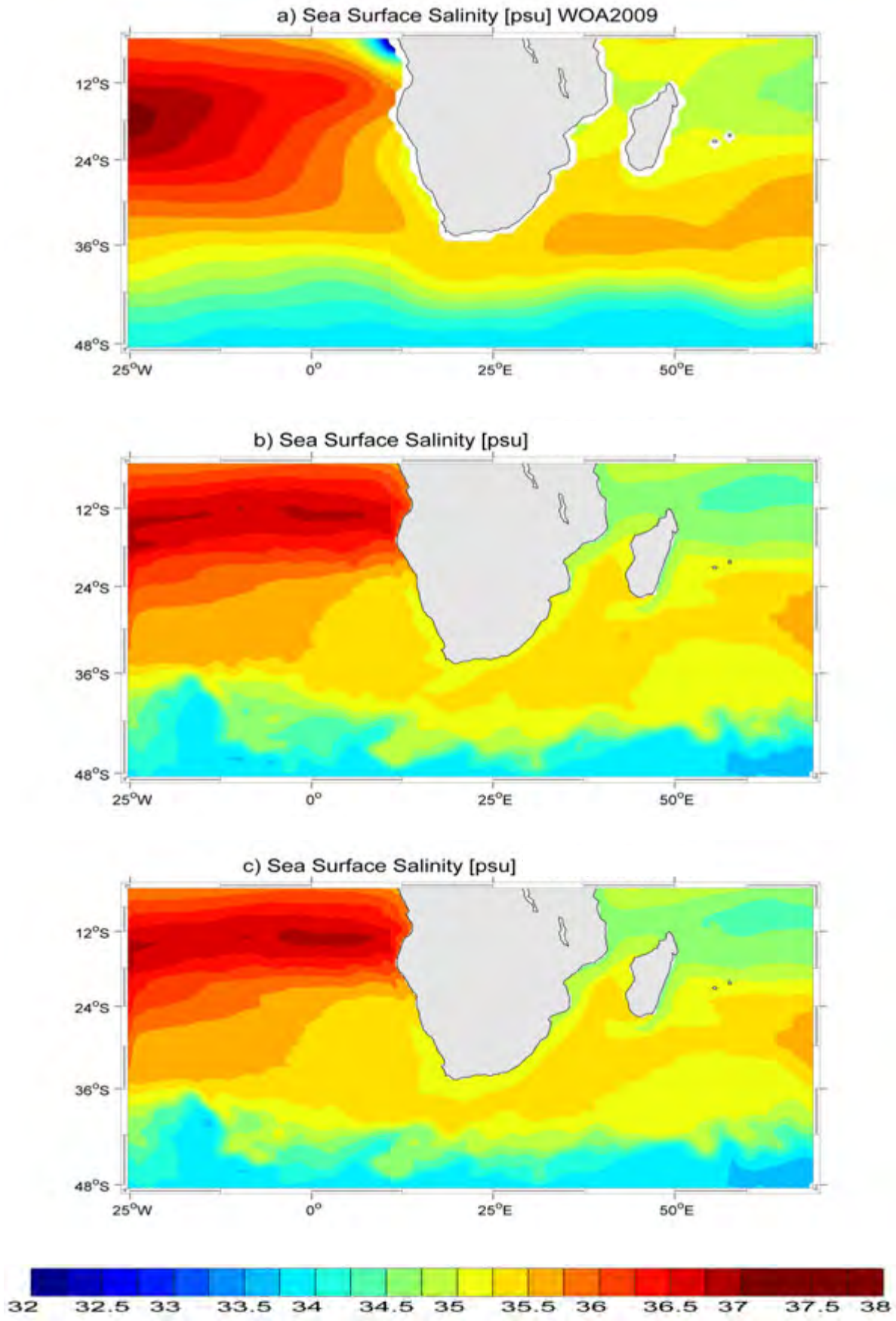

Figure 4.6 Mean Sea Surface Salinity (psu) of the domain for a) WOA09, b) Nested model and c) Standalone model data.

As in **Figure 4.5**, a further analysis of the monthly climatology is performed in four boxes, indicated in Figure **4.7a.** As expected, the salinity in the subtropical region is higher than the salinity in the SAZ. The two boxes in the STZ, A1 and B1 (**Figure 4.7b**) show the models underestimating salinity by ±0.25 in this region. In box A1, the models simulate similar surface salinity, whereas B1 indicates higher salinity (0.01 psu) during winter, spring and early summer for the nested model. The largest difference between the two model salinity occurs within the child domain.

In the SAZ box C1 shows both models underestimating the surface salinity by >0.5 psu. Box, D1, within the child domain, illustrates the models overestimating the surface salinity by ±0.25 psu for the nested model and ±0.5 psu for the standalone model.

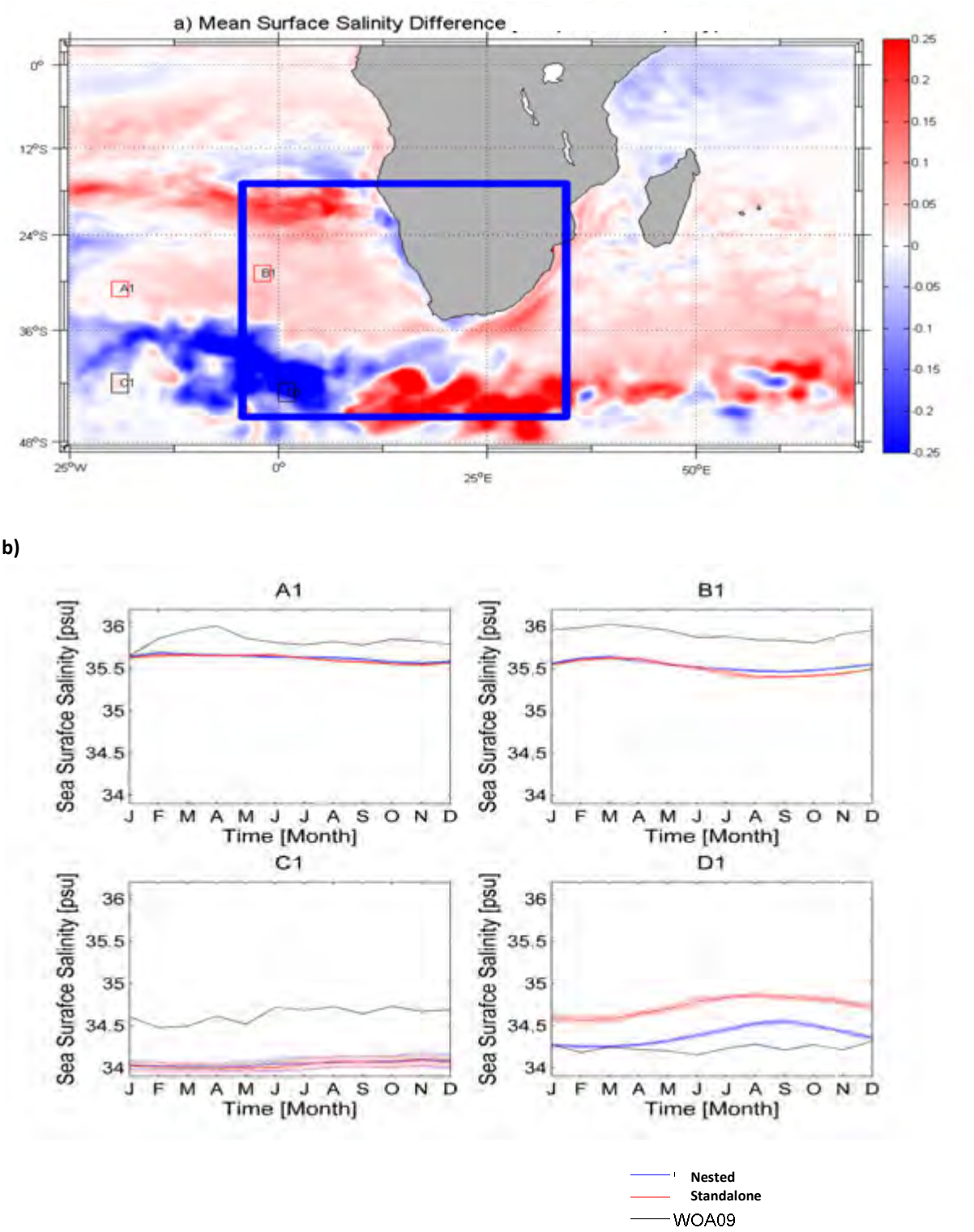

Figure 4.7 Mean Sea Surface Salinity (psu) a) Difference between the nested and standalone model. The blue box shows region where the child nest is located in the nested model and the smaller boxes represent regions chosen for further investigation and b) Time-series of monthly climatology for the four boxes.

4.4 T-S Diagrams for Four Boxes A1, B1, C1 and D1

The physical properties of a water column are determined by the water masses which are present. These water masses are defined by their physical properties such as temperature and salinity. The study domain contains five main water masses namely, Sub-Antarctic mode water, Sub-Antarctic surface water, Antarctic intermediate water, deep water and Antarctic bottom water as seen in **Figure 4.8**. **Figure 4.8** shows the various water masses in profiles done in the Atlantic and also the Southern Ocean.

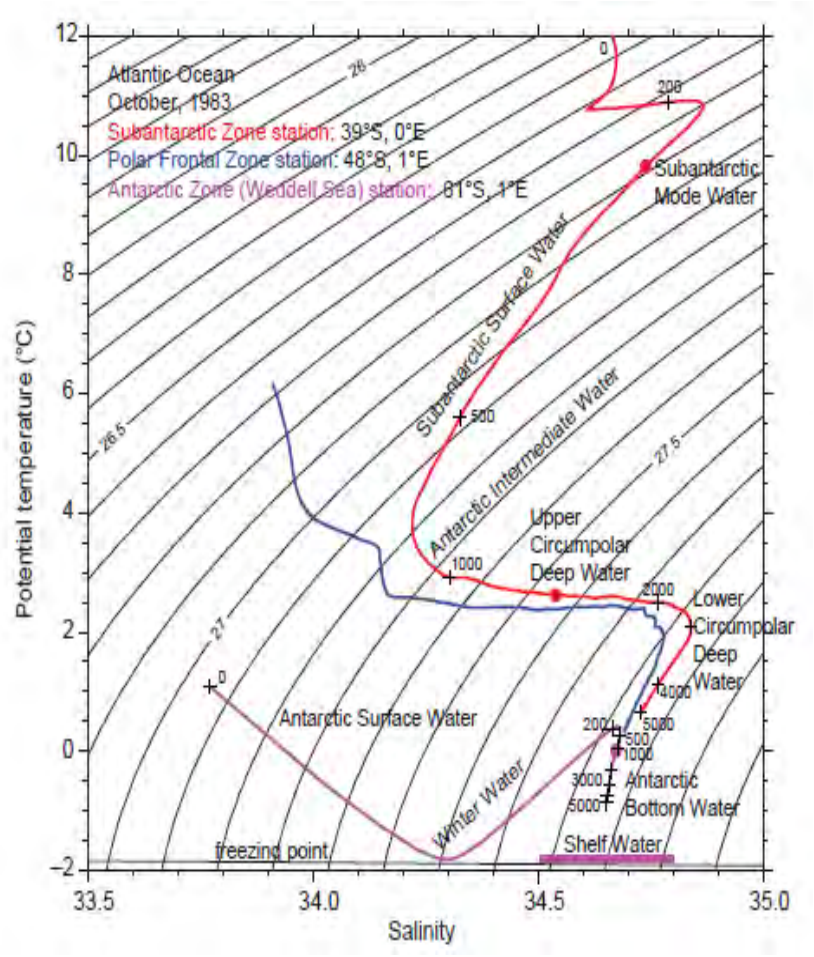

Figure 4.8 Water masses in South Atlantic (Adapted from Talley et al., 2011)

This section uses both the nested and standalone data as well as WOA09 data to identify the water masses.

The T-S diagrams for boxes A1 and B1 (**Figure 4.9**) have four water masses present namely Sub-Antarctic surface water, Antarctic intermediate water, deep water and Antarctic bottom water. The surface water in these diagrams is of lower density in both sets of modelled data. This lower density is a result of lower surface salinity in the modelled data. The models have intermediate water with higher density due to higher salinity concentrations. The deep water in these diagrams shows minimal differences between the modelled and observed data. Bottom water is only present in the modelled data in A1. The nested model simulated water properties closer to observed data. The model data deviates more from observed data in B1.

C1 and D1 T-S diagrams (**Figure 4.9**) are the boxes within the SAZ. C1 has model surface and intermediate water with lower density. The T-S diagram for box D1 (**Figure 4.9**) shows the highest differences between the three datasets. The density differences arise due to the increased salinity in the models. The biggest difference in temperature and salinity data is seen between the observed and standalone model data.

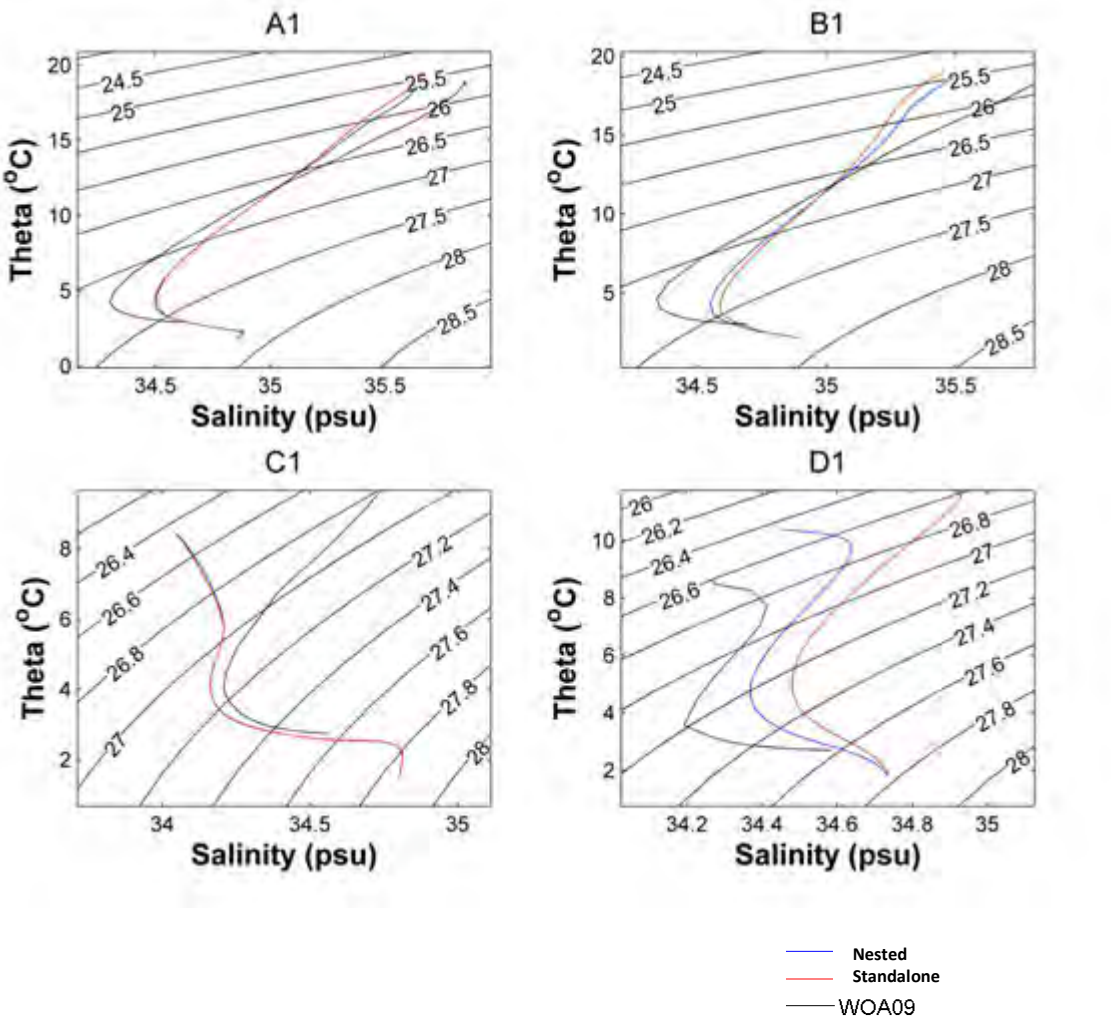

Figure 4.9 Mean Ocean Potential Temperature [°C] – Salinity [psu] diagrams for four (As shown in Figure 4.7a) boxes within the domain. The T-S plots show observed WOA09 data, nested model data and standalone model data.

Conclusion

The outputs of the ROMS based configuration for the nested and standalone model have been compared to climatology datasets. The interannual simulations have been specifically set up to analyse the effect a child domain of increased resolution over the southern African boundary currents would have on the MLD in the South Atlantic and Southern Ocean.

This section focussed on analysing the ability of both the nested and standalone model to simulate the variables which influence the MLD. The variables analysed are the mean geostrophic surface flow, SST, Sea Surface Salinity, Water masses (from profiles), surface winds and surface net heat flux [Appendix A].

When the mean geostrophic flow of the models was compared to the new CLS-CNES09 product, the models accurately simulated most large scale flow in the domain. Slight differences occurred. The models had a more intense flowing SEC, a weaker AC, weaker ARC and a weaker Agulhas retroflection. The standalone model showed an unclear and widespread retroflection region. The next step was to compare the model westward transport, Agulhas leakage, to literature. The nested model showed a leakage close to literature values, whereas the standalone model has an Agulhas leakage nearly double the volume of the literature. This increased leakage developed due to a weaker retroflection, which would normally allow for a weaker ARC.

The SST of the domain was compared to Pathfinder SST climatology. The SST of the models captured the large scale features correctly. The models did, however, show larger areas of increased SST in the Indian Ocean and the Atlantic Ocean. The models also have increased SST in the SAZ, this results due to the increased Agulhas leakage in this region. Upon further investigation, the largest bias of SST is found in the SAZ within the child domain. The standalone model has a larger increased SST bias in this region; this bias is corrected in the nested model due to the presence of the child domain and the increased grid resolution.

The surface salinity was compared to WOA09 climatology. The models correctly simulate most large scale features but fail to simulate the presence of the Indian Ocean subtropical surface water. This leads to decrease in salt concentration in the water leaked into the South Atlantic Ocean.

Further investigation shows the surface salinity being higher in the observed WOA09 data, for boxes A1, B1 and C1. Box D1 is situated in the low salinity region for observed data, but due to the weaker retroflection in the region the water leaked into the South Atlantic reaches further south. Therefore, box D1, closest to the retroflection has a higher salinity than that of C1, which lies within the SAZ but is further from the child domain and retroflection region. The salinity of the standalone model has the highest concentration due to the increased leakage.

Water masses which were identified in the observed data were present in the model data. The water masses were, however, less dense in the surface for boxes A1 and B1. Box C1 showed the entire water column being less dense than that of the observed data. Box D1, as before, showed the biggest difference in density between observed data. Once again the standalone model had the largest difference between observed data and the differences in density were mainly a result of salt concentration.

The difference in model SST and SSS arise due to the differences in transport, Agulhas Retroflection position as well as eddy activity, which is a result of the difference in resolution over the South African boundary currents.

Chapter 5

RESULTS

The focus of this chapter is to define the positions of the Sub-Tropical Zone (STZ) and the Sub-Antarctic Zone (SAZ) in both model and observed data. It also examines the mechanisms driving the Mixed Layer Depth (MLD) in each of the models. The MLD climatology for each of the models is compared to the observed MLD climatology. Further analysis is performed to better understand what mechanisms drive the differences seen between observed and modelled data as well as the differences between the nested and standalone model MLD.

5.1 Defining Study Zones and Seasonality of MLD

5.1.1 Positions of STF and SAF

The positions of the STF and the SAF point out the location of the STZ and the SAZ. The mean ocean temperature of the WOA09, nested model and standalone model is used to locate the positions of the fronts based on the criteria described in chapter 3. The STZ is defined as the zone north of the STF, whilst the SAZ is situated between the STF and the SAF.

The STF for both the nested and standalone model is situated northward of the observed front; a substantial difference of the front position of up to 20^{o} latitude is seen in the Indian Ocean section of the domain (**Figure 5.1**). The difference in surface temperatures suggest that sub-surface water may also vary between models and thus result in a large difference in the position of the fronts due to the subsurface temperature criteria used to calculate position of fronts. The observed data shows a northward spike in the position of the front in the Agulhas Retroflection region, due to the influx of warmer Indian Ocean water in this

region. Both models capture this spike in the region but it is exaggerated by a northward shift of ±10^{o} latitude. The largest bias of the front position is seen in the standalone model data. While it is evident that the largest discrepancy of the STF position is found in the Indian Ocean, it is important to note that the main focus of this study is in the Atlantic Ocean. The SAF position is well represented in the modelled data. The modelled SAF contains small variations from the observed data, the maximum difference is >6^{o} latitude.

The next step is to analyse the MLD in the STZ and the SAZ, this is done by analysing six boxes within these zones. Two boxes are chosen outside the child domain to capture differences closer and further from child domain boundary. The four boxes inside the chid domain captures data inside the highly variable region, e.g. Agulhas retroflection, Benguela Current, Agulhas Return Current, etc. **Figure 5.2** shows the SST difference between the two models for 2010, it also shows the position of the nested child domain in the nested model (blue box) as well as the 2^{o}x2^{o} boxes selected for further analysis. In each of the zones, two boxes are positioned outside the child domain region while the remaining four boxes are positioned within the child domain region.

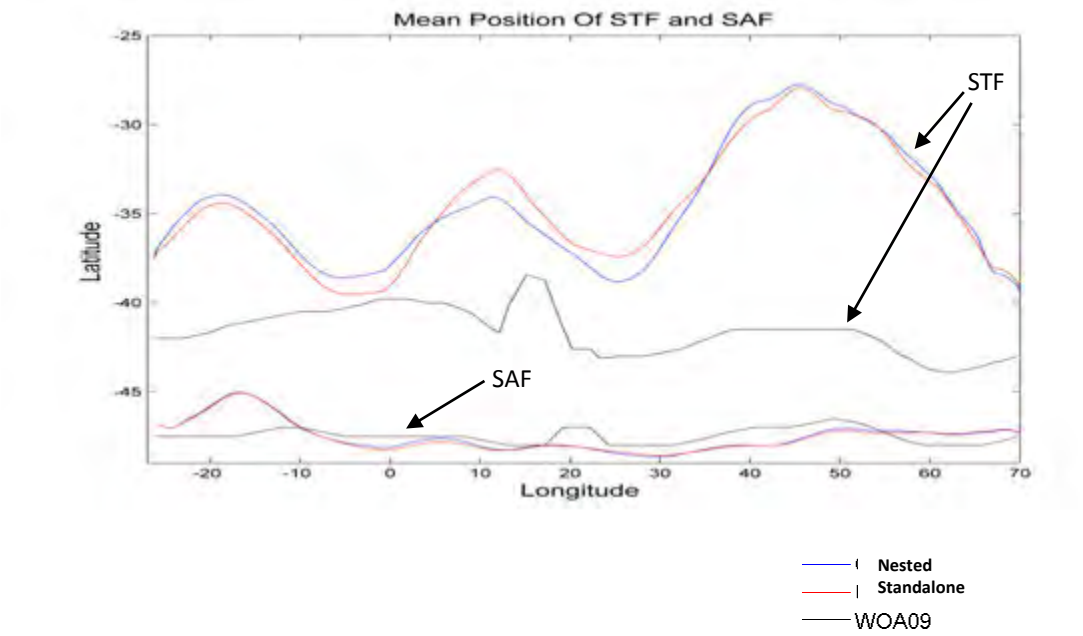

Figure 5.1 Mean position of STF and SAF for observed data, nested model data and standalone model data in the study domain.

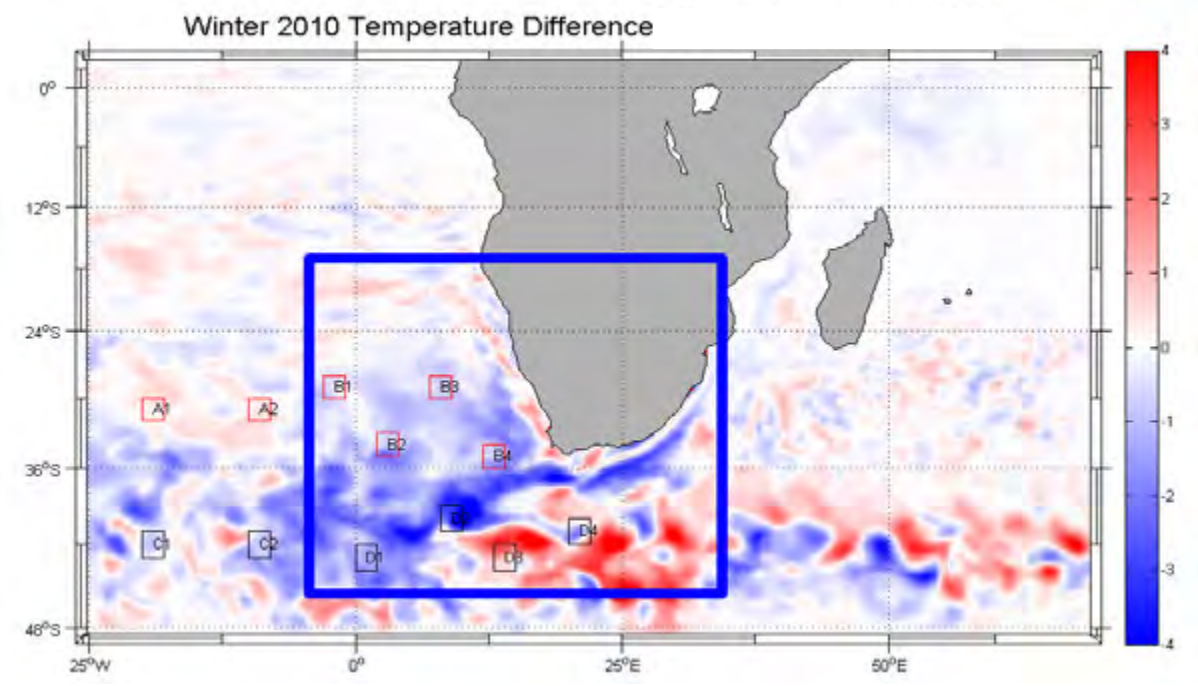

Figure 5.2 Winter SST difference between nested and standalone model (Nested – Standalone). The figure also shows the location of the child domain (blue box) and the smaller boxes for further analysis in the STZ and SAZ.

5.1.2 Seasonality of MLD climatology

The MLD calculated from model data is compared to two observed climatologies. The observed datasets used is the ARGO MLD (Hosoda et al., 2010) climatology for the period 2005-2009 and the de Boyer Montégut et al. (2004) MLD climatology. It is evident that both the nested and standalone model is able to simulate the seasonality observed in the domain.

In the STZ both the nested and standalone model MLD (**Figure 5.3a**) is deeper than that of the observed MLD. The break in stratification occurs between March and April in this zone. The maximum MLD is seen between August and September, whilst the spring restratification starts during September. It is evident that the models overestimate MLD during winter. Modelled MLD in areas outside the child domain (A1 and A2) is overestimated by ±150 m for both models whilst the areas within the child domain region (B1, B2, B3 and B4) overestimate MLD by ±100 m for the nested model and ±125 m for the standalone model. These overestimations of MLD may be a result of increased turbulence in the region as well as the mixing scheme used in the model setup, these in turn may affect the biogeochemical cycles of models. Mechanical inertia of the water column may be increased due to overestimation of salinity and temperature resulting in deeper MLD.

The MLD in the SAZ (**Figure 5.3b**) is deeper than in the STZ. The models simulate seasonality similar to that of the seasonality observed in the region. Both of the models tend to overestimate MLD in this zone, particularly during winter months when strong mixing occurs in the models. In this zone far from the child domain (C1) both models simulate MLD close to the observed MLD. The models also show stratification occurring one month earlier than that observed in the domain. Closer to the child domain the models both overestimate MLD during winter by 100 m for the nested model and 120 m for the standalone model. Moving into the child domain region the models both show a substantially deeper MLD (D1, D2, D3 and D4) than that observed in this region. While the models simulate MLD deeper than the observed data it is important to note that the largest difference is still seen during winter. The modelled data shows a slope with a steeper gradient leading to the deep MLD captured during winter; this may be the result of a weaker stratified water column in the models. The nested model does however present winter MLD closer to the observed MLD in this region,

with a max difference of 240 m whilst the standalone model presents a maximum difference of 390 m in the SAZ (box D1).

In summary, both models capture seasonality fairly well in the STZ and the SAZ. The nested model overestimates MLD but is still much closer to the observations than the standalone model. The use of the child domain with increased resolutions leads to differences in the physics in the models which would quantify the differences seen between the modelled data, especially during winter months.

a)

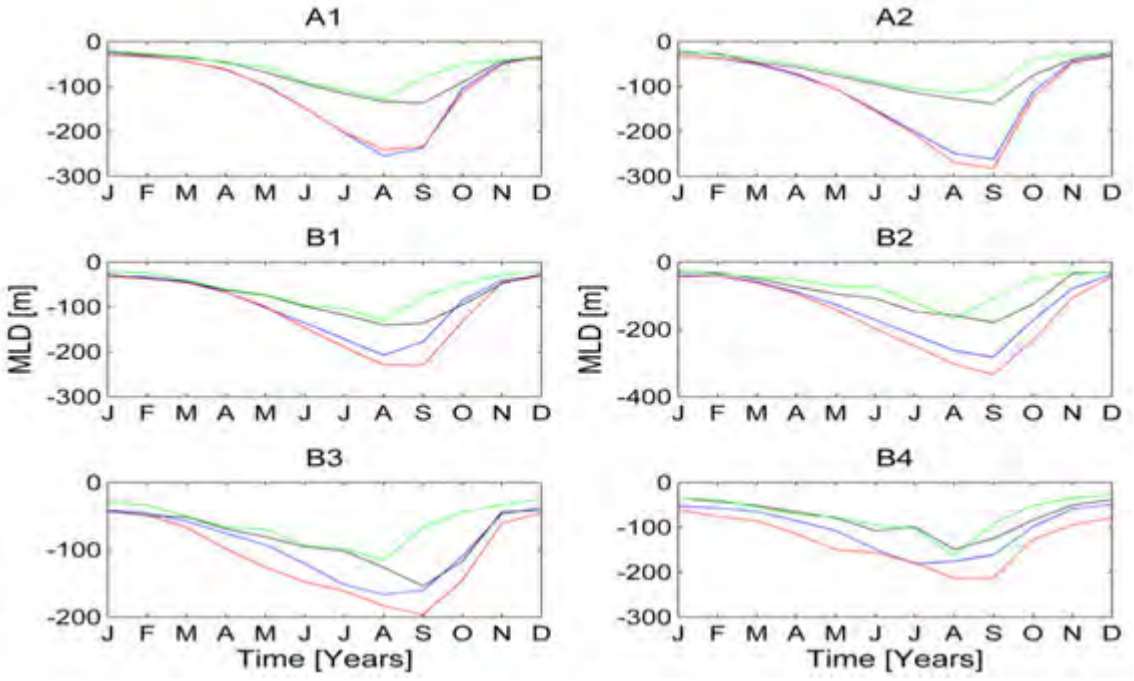

b)

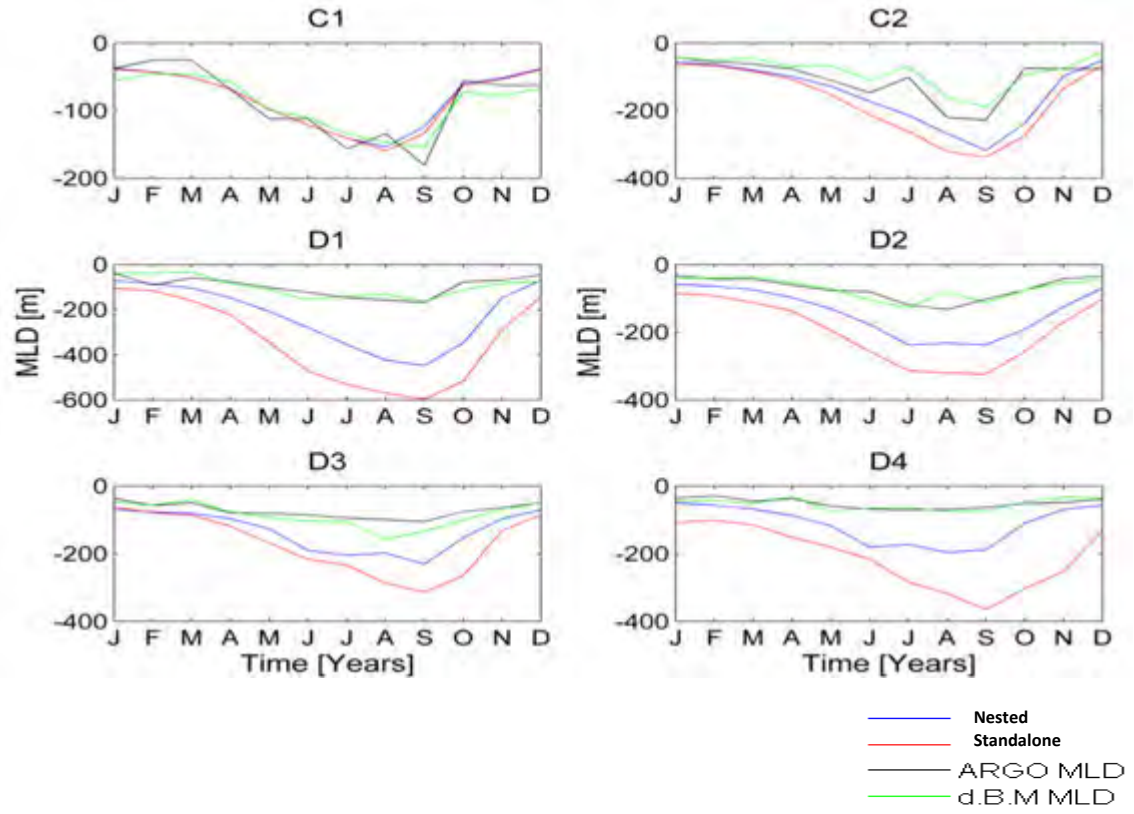

Figure 5.3 Mixed layer depth (MLD) in each of the boxes for modelled and observed climatology data for a) STZ and b) SAZ.

5.2 Nested and Standalone model comparison

The difference between the nested and standalone MLD is further investigated in this section. Each of the boxes shown in **Figure 5.2** is analysed for the simulation period, 2005 to 2010.

5.2.1 Time-series Analysis

In the STZ, the models both follow a similar seasonal cycle throughout the six-year simulation (**Figure 5.4a**). In the area outside the child domain, the models simulate MLD without any significant differences between the two models. In areas further from the child domain (box A1) the largest difference between the models is observed when the nested model MLD is <20 m deeper during certain years whilst areas closer to the child domain (box A2) show the standalone model MLD is 50 m deeper than that of the nested model MLD during certain years. Moving into the child domain area the MLD of both the nested and standalone model shows increased intra-seasonal variability. Throughout the six years, the models simulate comparable spring and summer MLD. During winter, the standalone model MLD is deeper than that of the nested model, with differences reaching up to 120 m in some areas. Even though the winter mixing of the standalone model is deeper it is noted that the slope of the standalone model MLD is much steeper than that of the nested model during certain years, this leads to similar MLD during the spring and summer months. In this case a steep slope indicates rapid change in MLD or rapid weakening in water column stratification. It is evident that these differences (e.g. B2 during 2008, B3 during 2008 and B4 during 2007) are a result of the difference in horizontal resolution in the models.

The intra-seasonal variability in the SAZ is much higher (**Figure 5.4b**) than that observed in the STZ. Both the models follow the same seasonal cycles in most of the areas. The largest discrepancy in the model seasonal cycle is seen in regions closer to the Agulhas retroflection, e.g. D4. As with the STZ, the regions further from the child domain shows little differences between modelled MLD, with the largest difference seen in box C2 where the standalone model has a winter MLD 50 m deeper than that observed in the nested model. Within the child domain, the standalone model MLD remains deeper than the nested model MLD throughout the year, with some exceptions (e.g. D4 during 2009 winter). On one occasion (D3 2005) the ML of the standalone model continues to deepen whilst the nested

model begins with its spring restratification thus showing a mismatch of the seasonal cycle during that year. The difference between the two models ranges from 1 to 40 m during summer and 5 to 200 m during winter within this region. During the break of stratification, the standalone model MLD has a steeper slope than observed in the nested model. The gradient of this slope becomes more relaxed during spring restratification resulting in the deeper MLD observed in the standalone model during spring and summer.

In conclusion, the MLD analysis in the regions further from the child domain show low variability and small differences between the MLD of the standalone and nested model. Moving towards the child domain the MLD of both models show increased intra-seasonal variability. In most of the years, the standalone model shows a deeper MLD, especially during winter.

a)

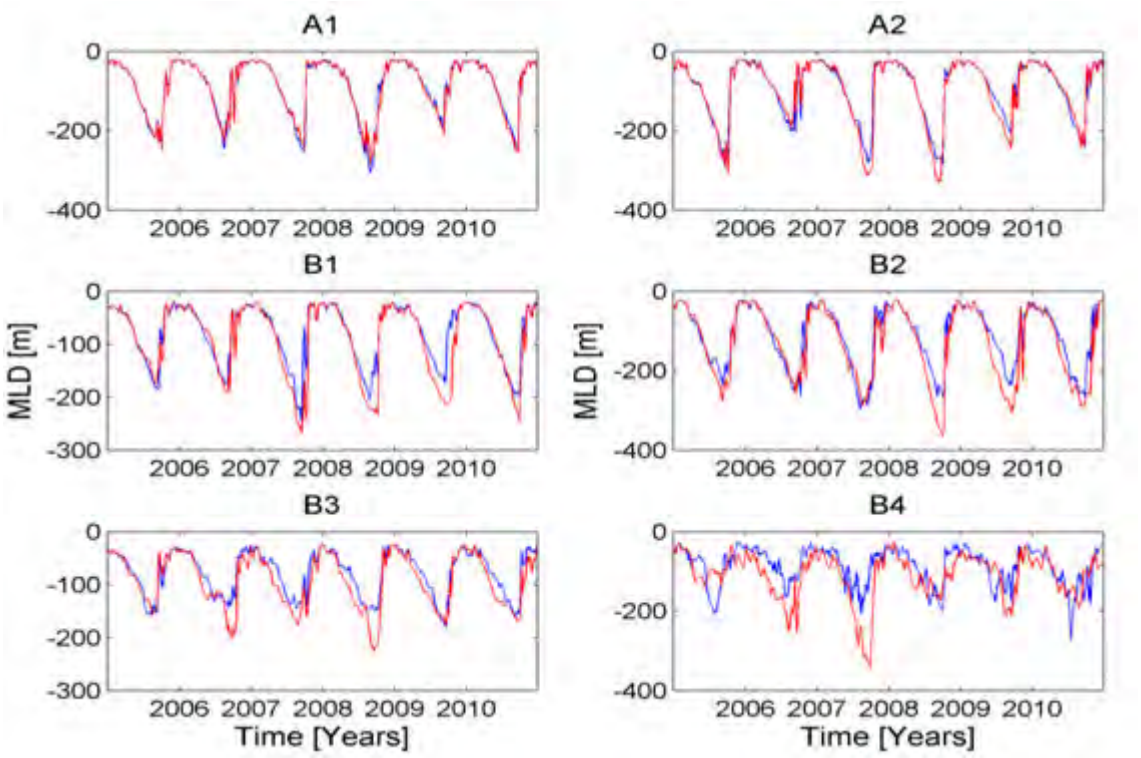

b)

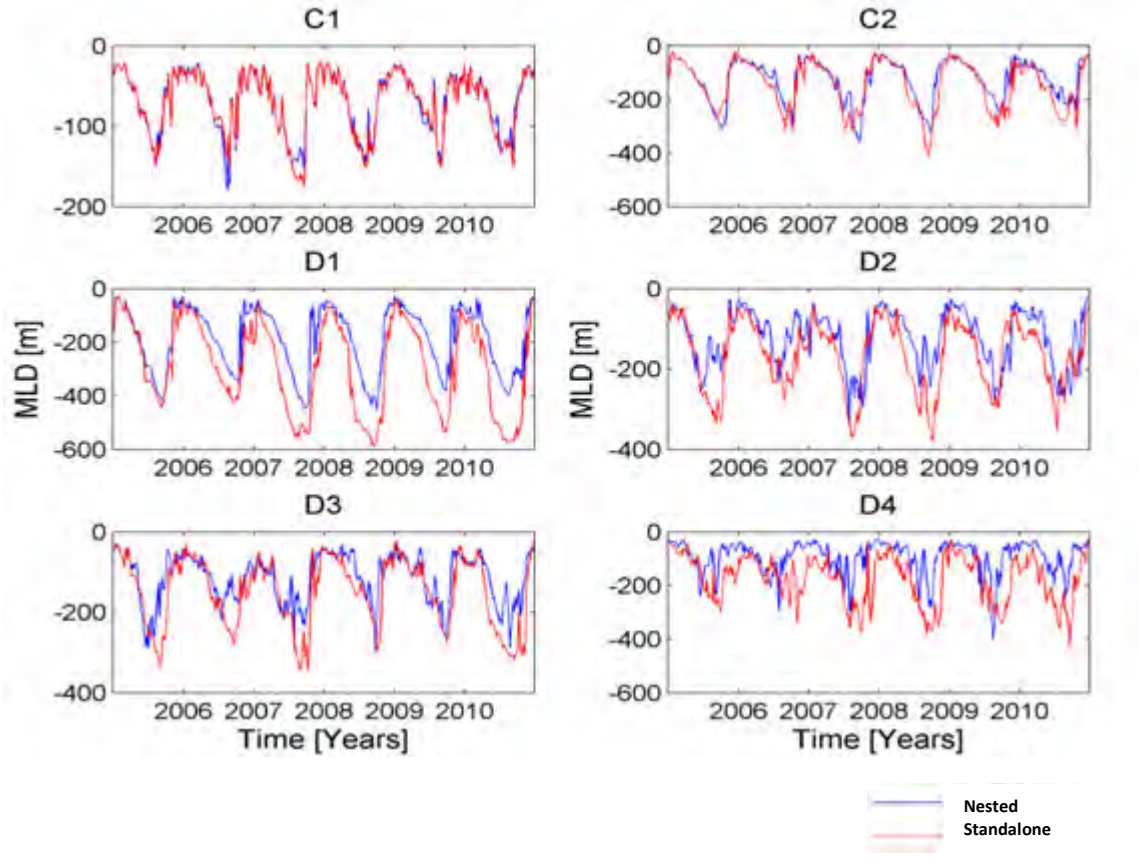

Figure 5.4 Mixed layer depth (MLD) six year time-series for each of the boxes for the Nested and Standalone model data for a) STZ and b) SAZ.

This section analyses regression plots in **Figure 5.5**. A regression analysis allows for the comparison between the nested and standalone model MLD variability.

The linear regression values outside the child domain remain well above 80%, with some areas reaching 97%. Inside the child domain, the values drop drastically from 97% to 36% in the STZ and 85% to 29% in the SAZ; the lowest values are seen closer to the Agulhas retroflection. The values in Table 5.1 point out the correlation between the nested and standalone model MLD. The strongest correlation value is observed outside the child domain (r=0.98) whilst the weakest correlation is observed inside the child domain (r=0.54). From the regression and correlation, it is clear that a large bias exists in the area within the child domain. The largest bias is seen in regions close to the Agulhas retroflection region, for both the STZ and the SAZ. This suggests that the models show larger differences in MLD in regions within the child domain.

Table 5.1 Correlation values for each of the boxes.

BOX	Correlation value (r)
A1	0.98
A2	0.97
B1	0.93
B2	0.94
B3	0.92
B4	0.60
C1	0.97
C2	0.90
D1	0.92
D2	0.79
D3	0.80
D4	0.54

a)

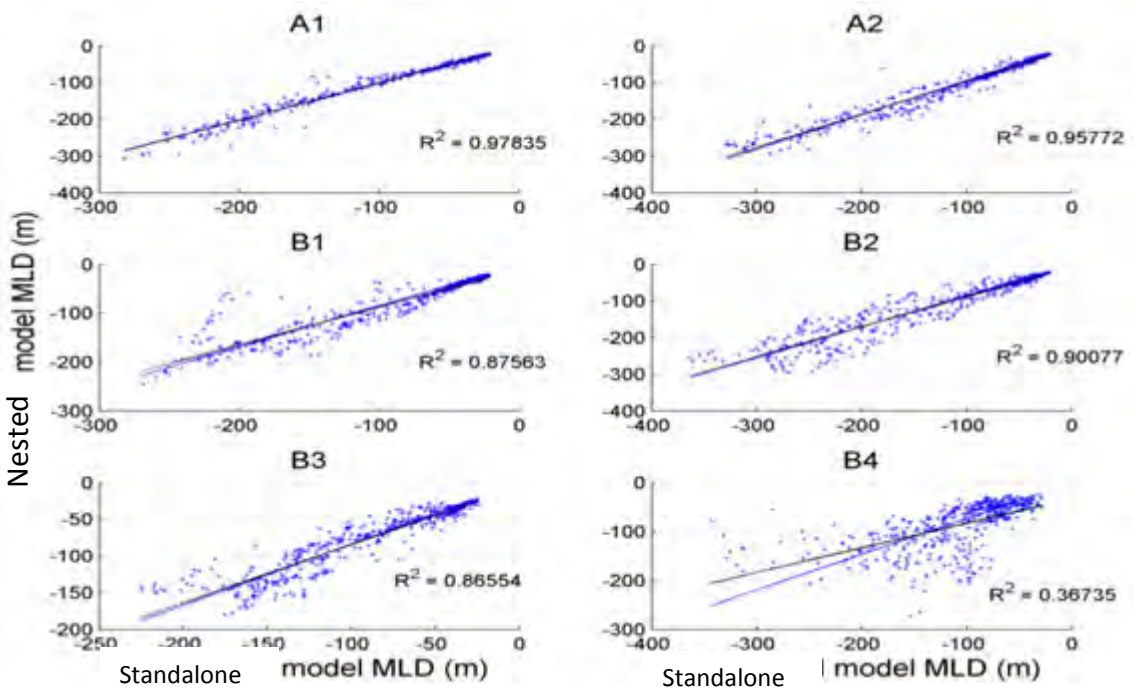

b)

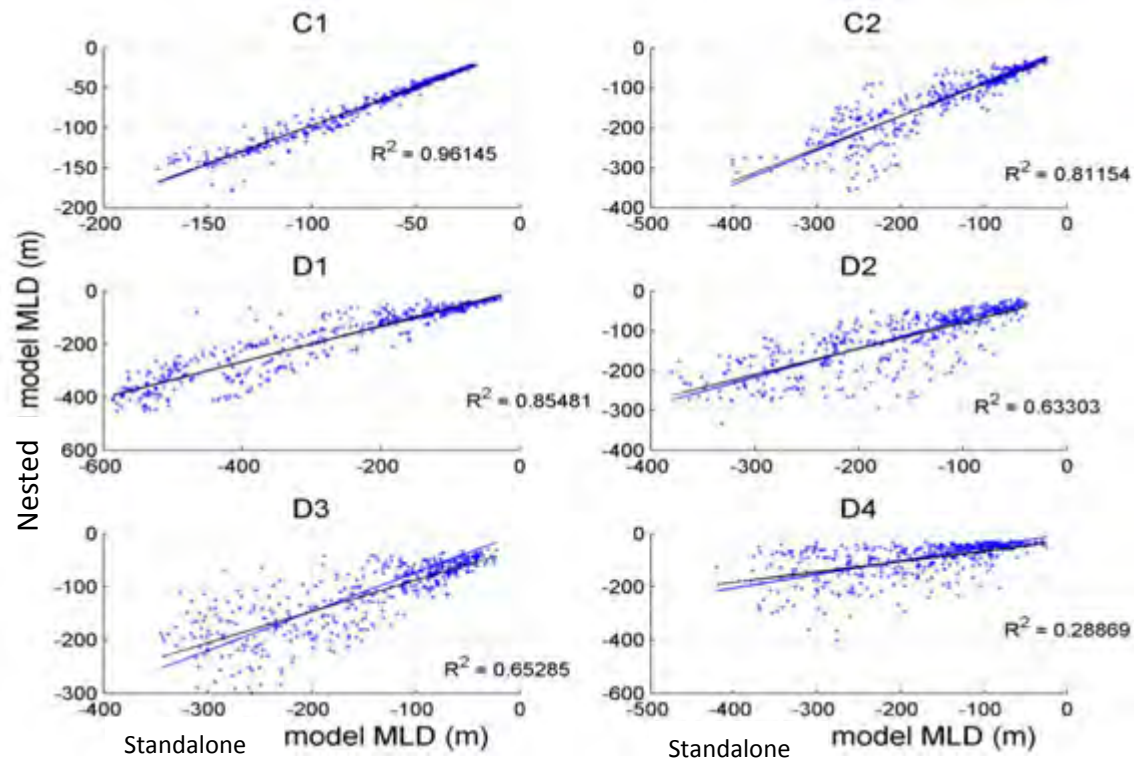

Figure 5.5 MLD regression plot for Nested and Standalone model data for a) STZ and b) SAZ.

5.2.2 MLD and RMS vorticity comparison.

The difference between modelled MLD is further examined by randomly selecting one of the six years in each box for additional analysis. **Table 5.2** show the selected years; the table shows three dates in the selected years for which vertical sections were analysed. The three dates chosen represent the break of the summer stratification, the deep winter MLD and the stratified water column. The selected dates are chosen based on the nested model data.

Table 5.2 Years and dates selected for further analysis for each of the boxes in the STZ and the SAZ

BOX	Year	Deepening	Winter MLD	Stratified
A1	2010	10 April	20 September	5 October
A2	2010	5 April	20 September	5 October
B1	2010	20 March	10 October	20 October
B2	2008	25 February	15 September	20 October
B3	2008	20 February	20 October	5 November
B4	2010	10 March	20 October	5 November
C1	2007	30 April	25 September	10 October
C2	2008	30 April	25 September	10 October
D1	2010	5 March	20 August	20 November
D2	2005	5 March	20 July	20 November
D3	2007	5 April	30 July	5 November
D4	2010	15 August	15 September	15 October

Figure 5.6 shows the MLD along with Root Mean Square Vorticity (RMSV) values for each of the models. RMSV is calculated by taking the square root of the sum of vorticity squared within each box. Using RMSV determine whether or not the presence of a mesoscale eddies plays a significant role in the difference observed in the MLD simulated by the nested and standalone model MLD simulations. These eddies, whether cyclonic or anticyclonic, play a role in the structure of the water column due to its downwelling and upwelling nature. Whether or not this influences MLD in the boxes is determined by analysing **Figure 5.6**.

In the STZ, the RMSV (**Figure 5.6a**) is $\pm 2.5 \times 10^{-5}\ s^{-1}$ higher in the standalone model in regions outside the child domain (boxes A1 and A2). This increased vorticity does not result in a large difference in MLD in this region. Inside the child domain, the difference between the nested and standalone model RMSV is more variable than outside the child domain, peaks of the RMSV coincide with the initiation of spring stratification. Areas closer to the Agulhas retroflection show maximum RMSV during spring in the standalone model.

In the SAZ the RMSV (**Figure 5.6b**) of the two models show small differences ($<5 \times 10^{-6}\ s^{-1}$) during most of the year; unlike the substantial differences observed in MLD. In some instances, the break in stratification in the water column is preceded by a peak in the RMSV in the standalone model. There are isolated events during which a peak in RMSV precedes the onset of spring stratification in the nested model.

The RMSV affects the MLD of the water column as is demonstrated in some instances, e.g. March in Box B3 the MLD increases and RMSV increases for the standalone model. The influence is not significant enough to be the only mechanism driving the differences observed between the modelled MLD. The results suggest that eddies may impact MLD in some cases but it's effect is not large enough to drive the differences between the two models.

a)

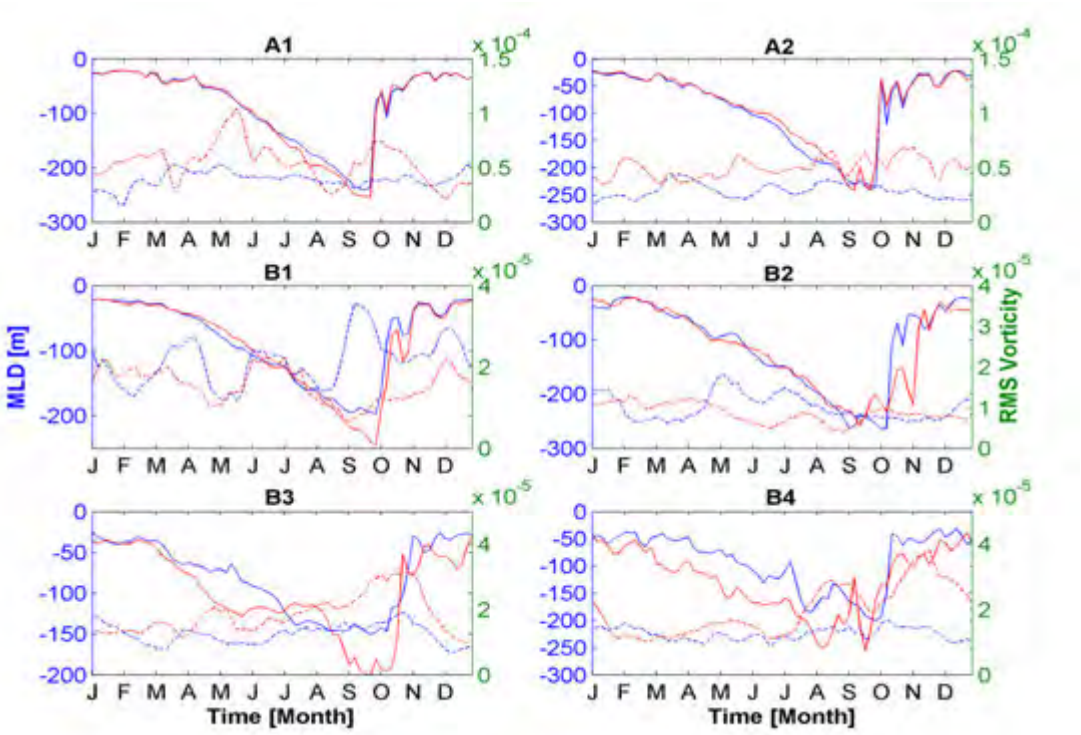

b)

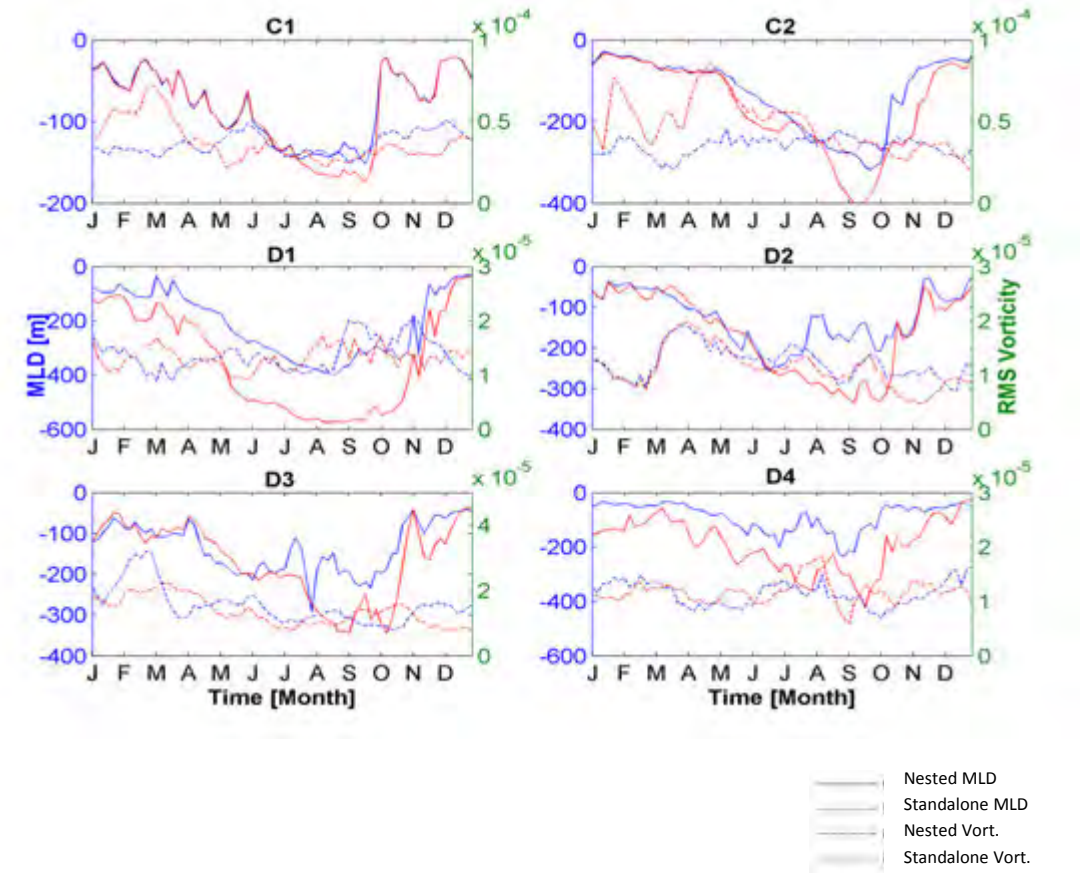

Figure 5.6 MLD (m) and RMS vorticity (s^{-1}) for years shown in Table 5.2.1 for boxes in a) STZ and b) SAZ.

5.2.3 Vertical structure of the water column

This section analyses the water column in each box to identify the mechanisms driving the difference observed in MLD between the nested and standalone models. The vertical sections are taken at the mid-latitude point of each box and include the entire longitude range of the box. Each of the sections is taken at the time-steps identified in **Table 5.2**.

Subtropical Zone (STZ)

Figure 5.7 shows the water column structure in areas outside the child domain, A1 and A2 (not shown), for both the nested and standalone model. The first panel of **Figure 5.7a** illustrates a uniformly warm (>22^{o}C) water column within the upper 100 m in both models. Below 100 m the isotherms in the standalone model indicates the presence of a weak cyclonic feature. The April MLD of the standalone model is driven by the presence of cyclonic and anticyclonic features. In September, it is clear that the stratified water column is enhanced by the presence of cyclonic features in both models. **Figure 5.7b** shows the Brünt-Väisälä frequency (BVF) in the water column, the strongest stratification is observed during summer in both models. The water column of the nested model is more stratified than the standalone model during both winter and spring. Despite the lower BVF observed in the standalone model, the MLD still coincides with the MLD observed in the nested model; suggesting that the stratification affects MLD differently in the standalone model.

In most of the areas inside the child domain, the MLD of the standalone model is deeper than the MLD observed in the nested model throughout the year. In **Figure 5.8a** [Box B1] the upper layers of the water column show uniformly distributed isotherms during summer, a steeper isotherm gradient is observed in the nested model. The summer BVF plots **(Figure 5.8b)** show a highly stratified water column in both models; the stratification occurs closer to the surface in the nested model, this coincides with the shallower MLD observed in the nested model, similarly in boxes B2, B3 and B4 (not shown). An intense deepening is observed during winter in both models (**Figure 5.8a**); the isotherms along with the isopycnals show that this well mixed layer extends deeper in the standalone model. An

example of this is captured in B1 on 10 October, where the 17^{o}C isotherm is shallower than 190 m in the nested model and deeper than 220 m in the standalone model. The shallower MLD observed in the nested model coincides with the presence of mesoscale features. While the nested model experiences spring restratification. The increased MLD is a result of incoming warm and salty water which promotes mixing, forming a well mixed upper water column. In other areas the presence of the cyclonic features promotes stratification in the nested model during spring, whilst anticyclonic features promote deeper well mixed layers in the standalone model. Overall the water column of the standalone model is less stratified than that of the nested model (**Figure 5.8b)**.

Sub-Antarctic Zone (SAZ)

In the regions outside the child domain (C1 shown in **Figure 5.9a**), the MLD observed in the standalone model is slightly (<10 m) deeper than the MLD observed in the nested model during summer (**Figure 5.9a**). The water column of the nested model reaches stratification at a more shallow depth due to the presence of a cyclonic feature (**Figure 5.9a**). During winter, the MLD is overall deeper in the standalone model. In regions further from the child domain (C1) the MLD differs by ±50 m, whilst areas closer to the child domain (C2, not shown) shows a difference of ± 100 m between the nested and standalone model. There is an influx of warm salty water in the standalone model water column; the high density water promotes mixing resulting in a deep isopycnal layer in this model. During September, the nested model SST is higher than the SST observed in the nested model. The MLD of the standalone model is however still deeper due to the higher salinity, resulting in an isopycnal layer deeper than the isopycnal layer observed in the nested model. Overall the BVF is higher in the nested model (**Figure 5.9b**), suggesting a more stratified water column.

The MLD is more variable within the child domain (**Figure 5.10 and Figure 5.11**). In all cases (D2 and D3 not shown) the MLD observed in the standalone model is significantly deeper with differences reaching up to 180 m during winter. After analysing the vertical sections within the zone, it is inherently clear that the discrepancy with the modelled data is due to a bias, which is mostly found in this region where the standalone model simulates surface temperatures and salinities higher than in the nested model (**Figure 5.10a**). The warmer and denser surface water of the standalone model promotes mixing. The nested model water still has more cyclonic features and thus a more stratified water.

Indeed, the MLD of the nested model coincides with BVF values >$5x10^{-5}$ s^{-2} whilst the MLD of the standalone model coincides with values lower than $5x10^{-5}$ s^{-2} in some instances. This observation suggests that stratification affects MLD differently in the standalone model within the SAZ.

It is evident that the difference between the models increases moving into to the child domain in both the STZ and SAZ. Anticyclonic and Cyclonic features do impact on the MLD of

the models and are more frequently found in the nested model. The largest discrepancy of MLD between the models is observed in areas with large SST and Surface salinity bias, mainly within the child domain. The largest MLD bias is observed in the regions closer to the Agulhas retroflection.

a)

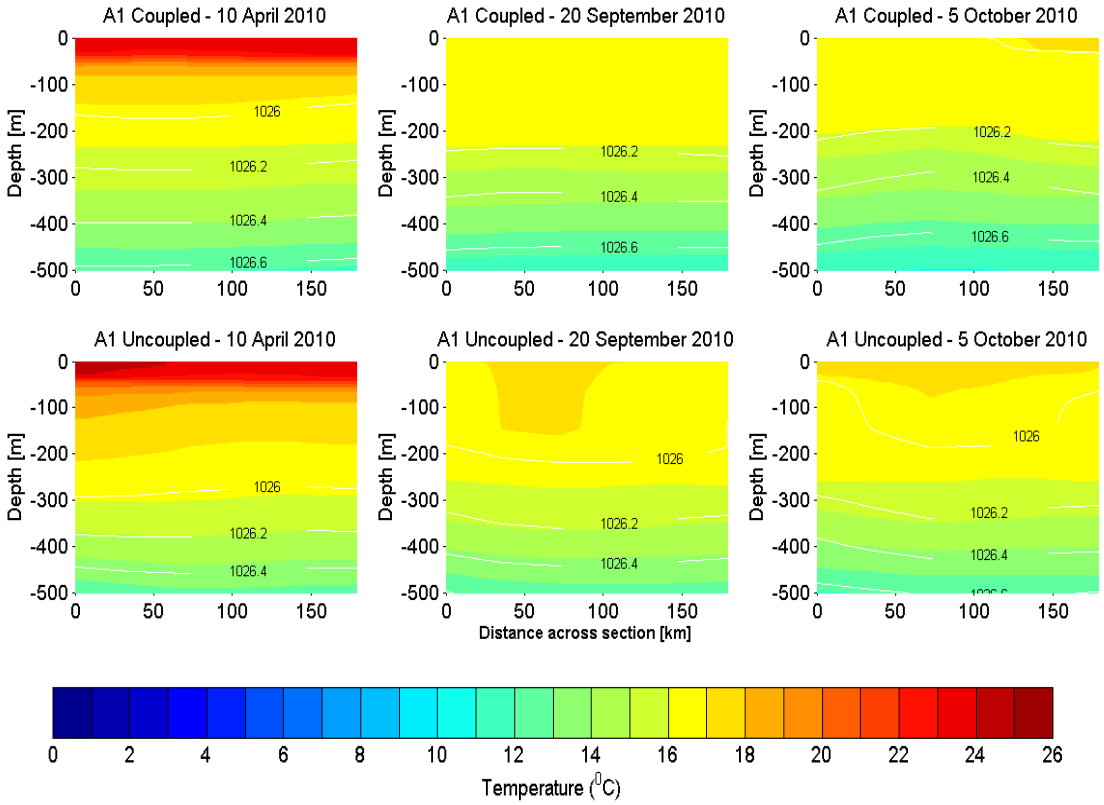

b)

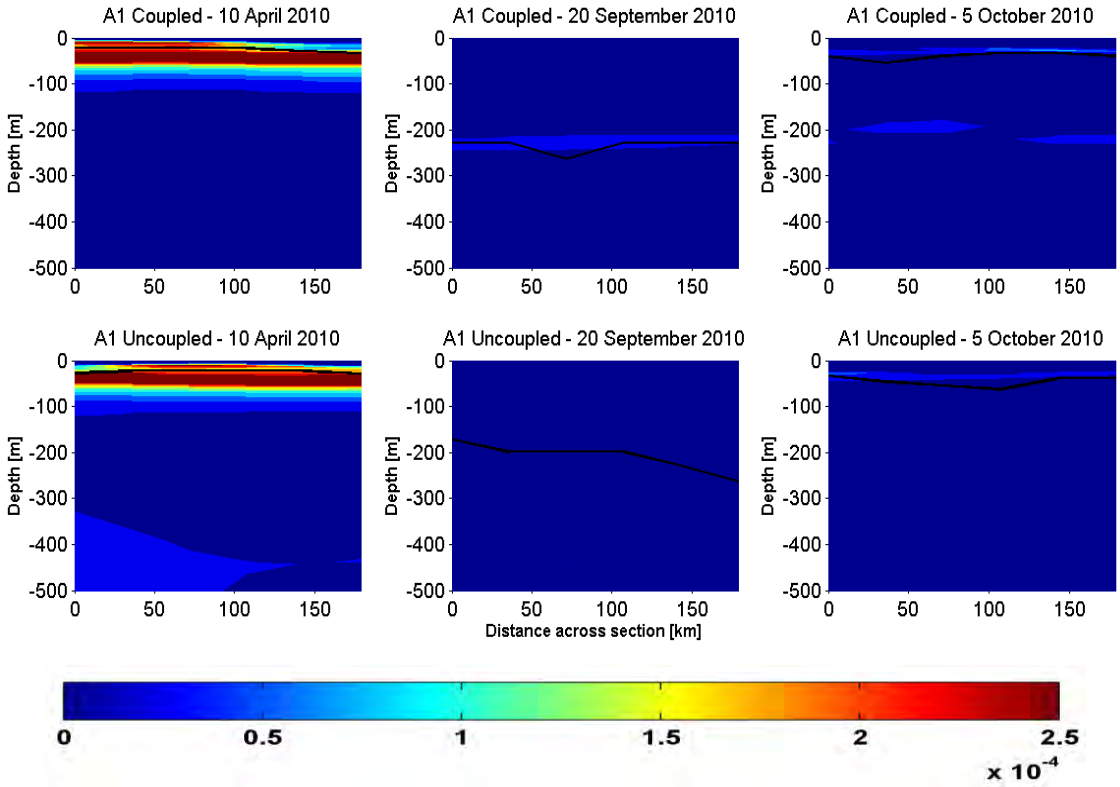

Figure 5.7 Vertical sections for three selected dates in box A1 for 2010, for a) Temperature (°C) and density (kg/m^3) (white isopycnals) and b) BVF (s^{-2}) and MLD (m) (black line).

a)

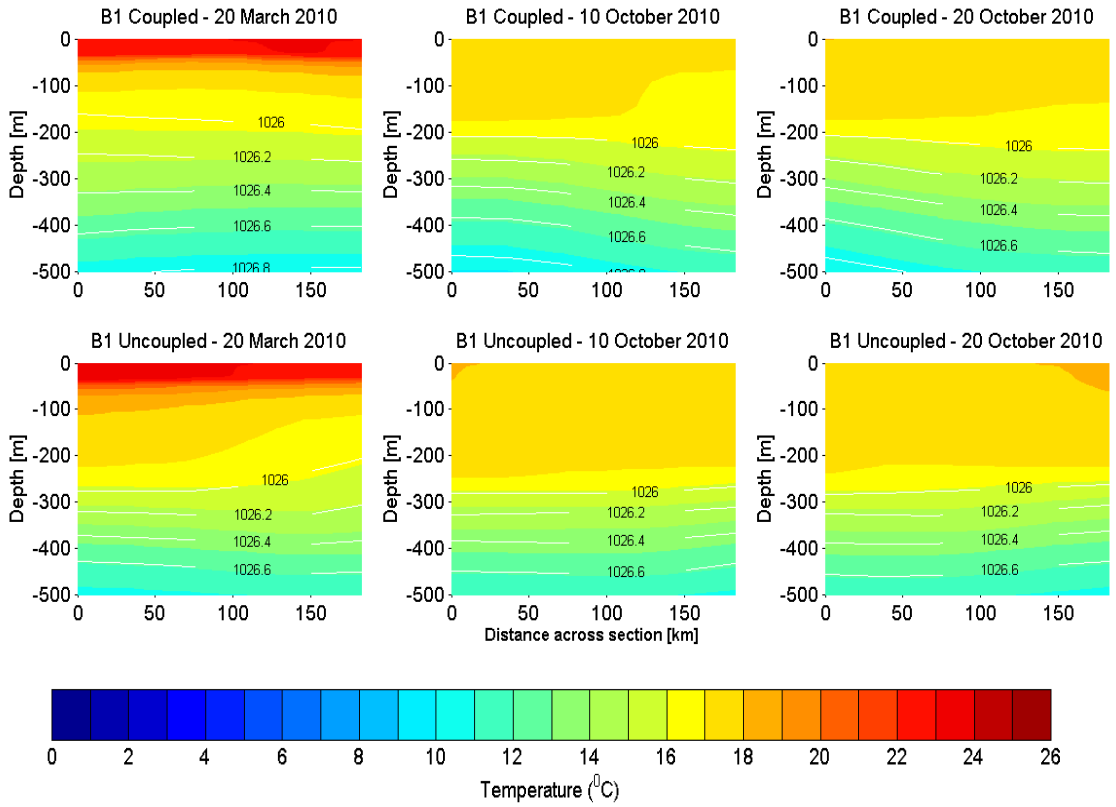

b)

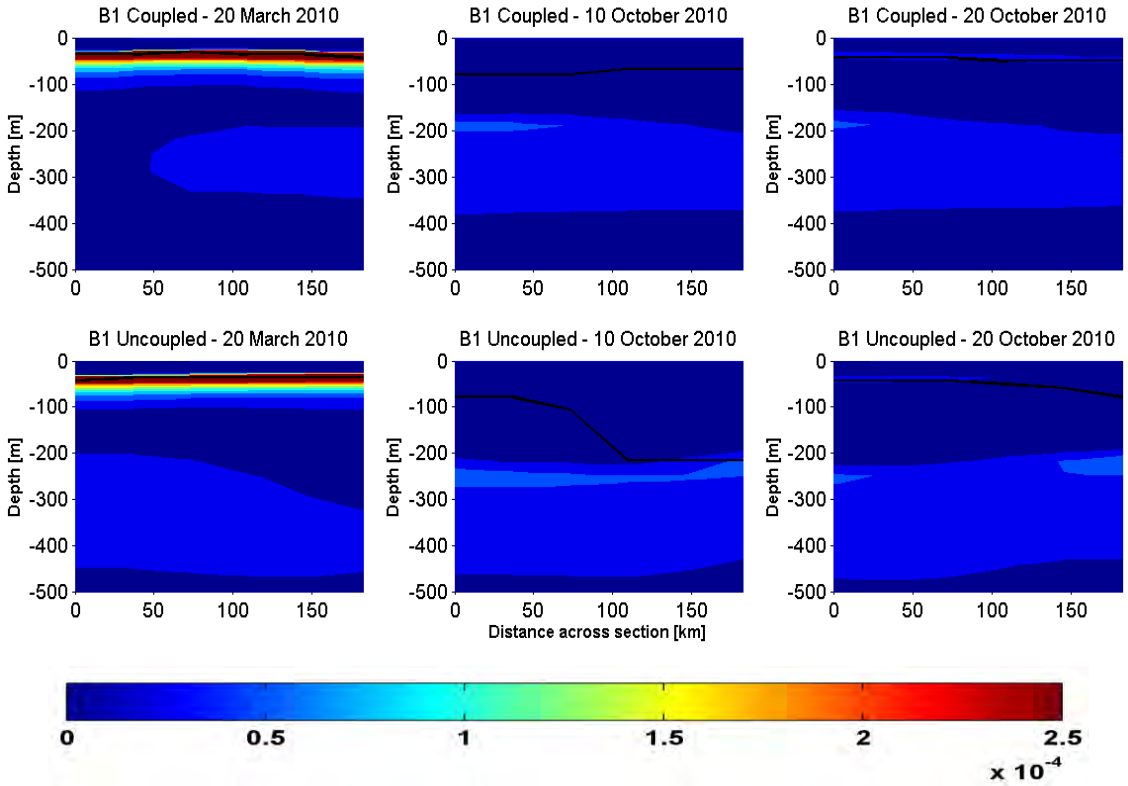

Figure 5.8 Vertical sections for three selected dates in box B1 for 2010, for a) Temperature (°C) and density (kg/m³) (white isopycnals) and b) BVF (s⁻²) and MLD (m) (black line).

a)

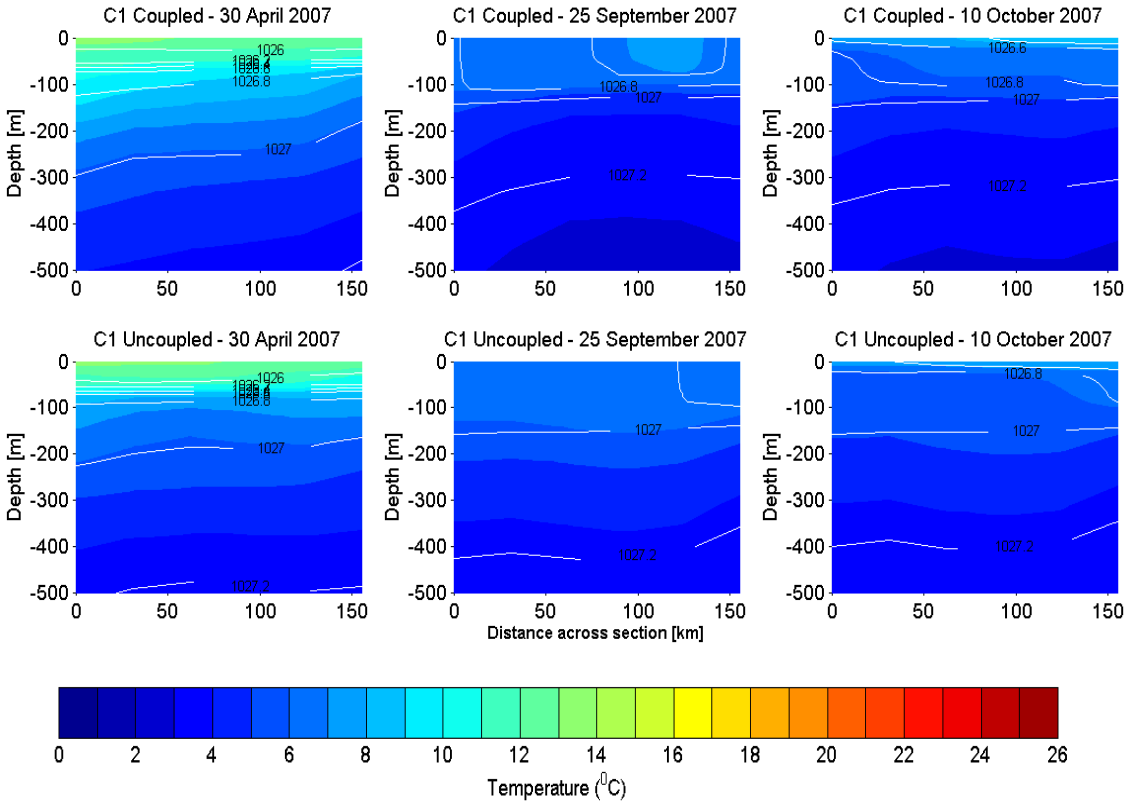

b)

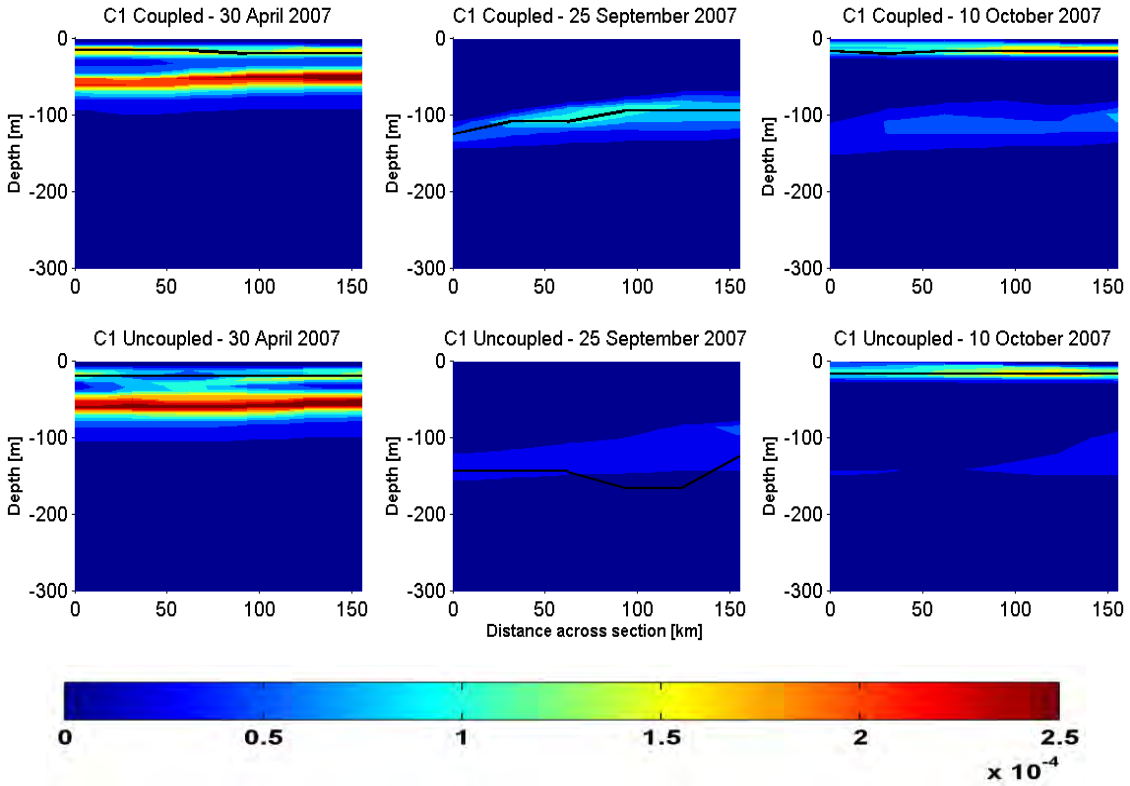

Figure 5.9 Vertical sections for three selected dates in box C1 for 2007, for a) Temperature (°C) and density (kg/m^3) (white isopycnals) and b) BVF (s^{-2}) and MLD (m) (black line).

a)

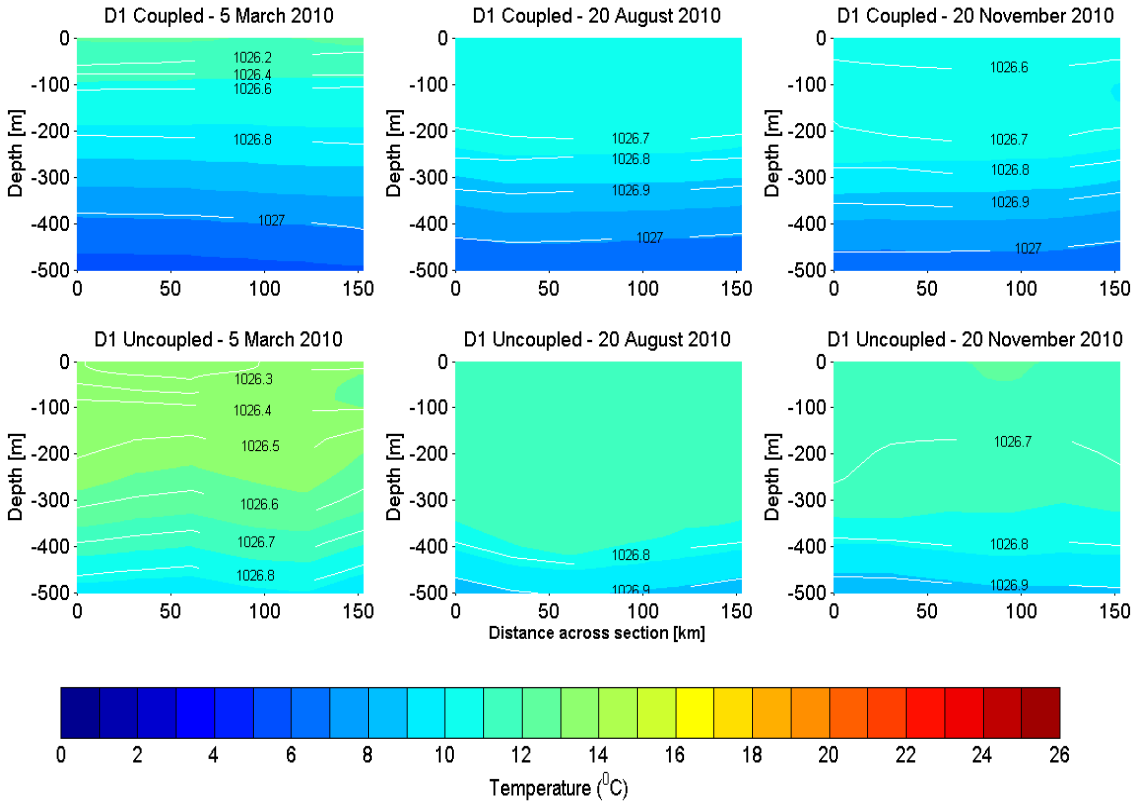

b)

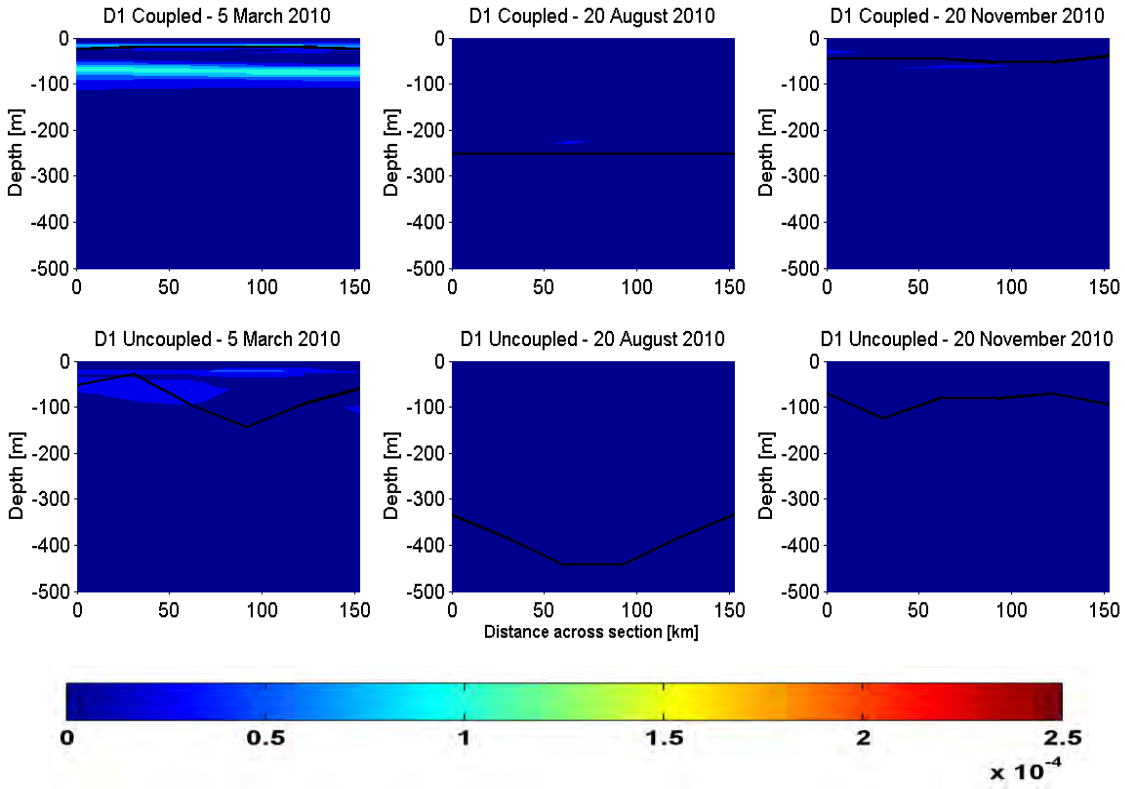

Figure 5.10 Vertical sections for three selected dates in box D1 for 2010, for a) Temperature (°C) and density (kg/m³) (white isopycnals) and b) BVF (s^{-2}) and MLD (m) (black line).

a)

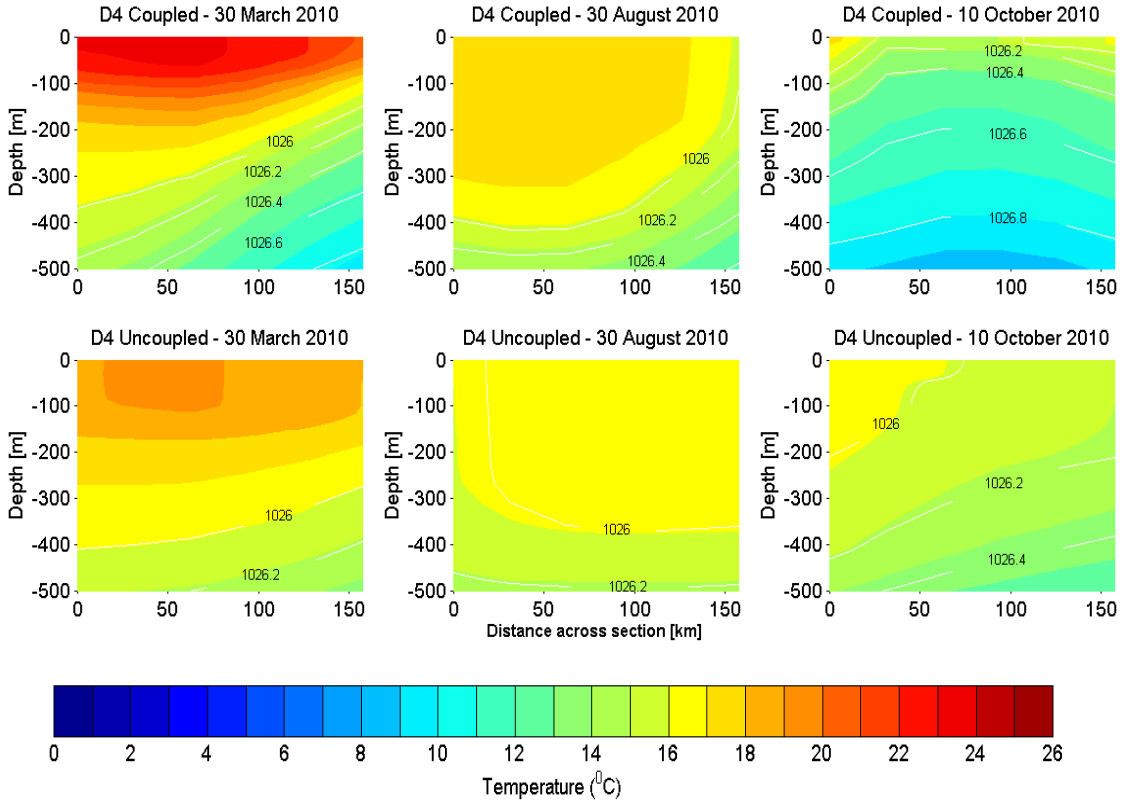

b)

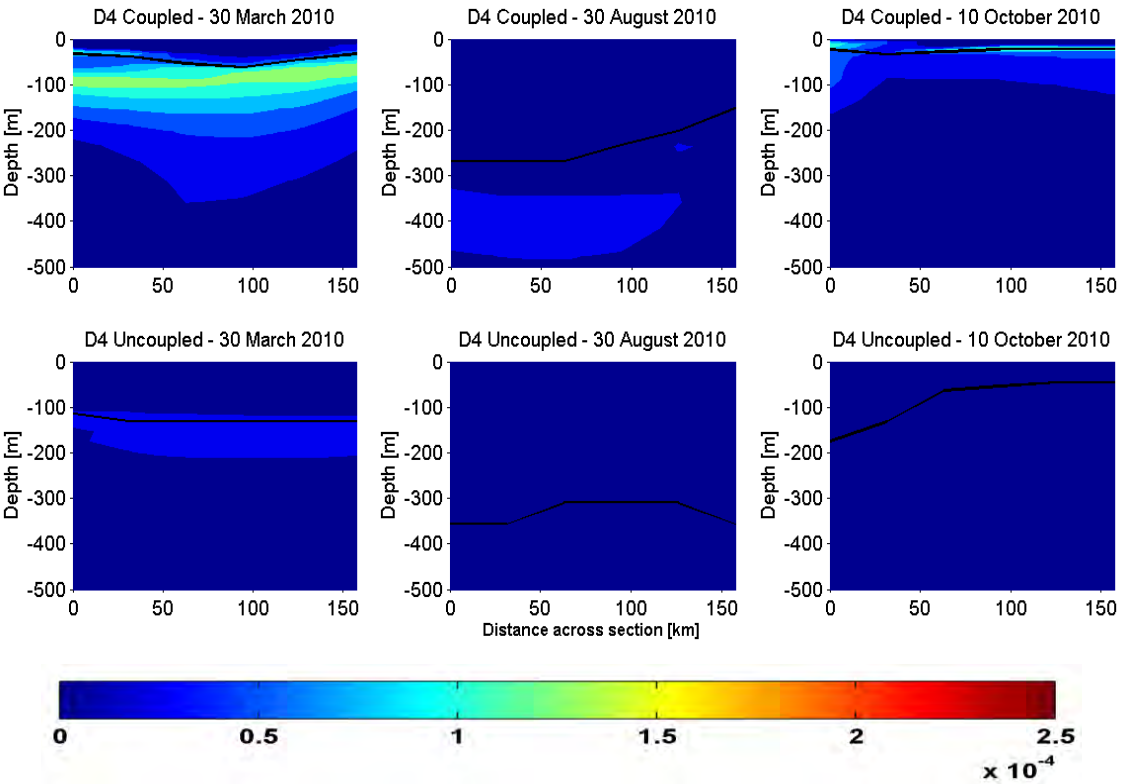

Figure 5.11 Vertical sections for three selected dates in box D4 for 2010, for a) Temperature (°C) and density (kg/m^3) (white isopycnals) and b) BVF (s^{-2}) and MLD (m) (black line).

Chapter 6

Discussion and Summary

In this project, we examine the MLD in the ocean using the Regional Ocean Modelling System (ROMS). The domain covers the Southwest Indian Ocean, Southern Ocean and the Southeast Atlantic Ocean. Two simulations are run; the first one is a 1/4^{o} resolution model with a nested child domain of increased resolution, 1/12^{o}, over the South African boundary currents (nested model). The second model is simulated at 1/4^{o} resolution throughout the domain (standalone model). Both models are interannual simulations, the nested model ran for 30 years while due to time limitations the standalone model ran for 6 years, 2005 to 2010. The analysis is based on data for 2005 to 2010 in the nested and standalone model.

6.1 Large Scale Flow and Mean State Physics

Analysis of the mean sea surface geostrophic flow revealed that the models are both able to capture the large scale flow illustrated in the observed CLS-CNES09 data (Rio et al., 2011). In the models the flow of the Agulhas Current is weaker than that in the observed data (**Figure 4.2a**). The largest difference in flow is in the Agulhas retroflection, which is slightly weaker in the nested model and very weak in the standalone model (**Figure 4.2**). The weaker Agulhas Current leads to more inter-ocean transport (Agulhas Leakage) (van Sebille et al., 2009). The standalone model shows increased Agulhas leakage of 23.18 Sv, nearly double the amount observed (15 Sv) in Gordon et al (1992). In recent years it has been found that Agulhas leakage has increased which may be a result of strengthening westerly winds (Loveday et al., 2015)

Analysis of the nested and standalone model physics reveal that the modelled SST and surface salinity is comparable with the observed salinity. The largest bias is seen in the southeast section of the domain (in the Indian Ocean) where both models underestimate surface salinity (**Figure 4.6**). The fresher Indian Ocean water is also observed in a model

study by Momin et al. (2014), with a lesser bias in the higher resolution nested model. In general, the models underestimate SST and salinity in the STZ and SAZ; except in regions closer to the Agulhas retroflection. Loveday et al. (2015) found that increased Agulhas leakage results in warming and increased salinity which explains the salinity and temperature bias found in the nested and standalone model. Vertical profiles show that both models are able to simulate the water masses in the STZ and SAZ, with lesser bias seen in the nested model.

Despite model difficulties in reproducing some oceanographic features in the region, the overall performance of both the nested and standalone models suggests that the model can be used to study the mixed layer processes in the South Atlantic.

6.2 MLD within the STZ and SAZ

Modelled mixed layer depth is currently overestimated by 10 to 30% in global ocean models (Juza et al., 2012). Mesoscale and sub-mesoscale resolving models are required to understand the sensitivity in the MLD dynamics (Swart et al., 2015). In a study by Levy et al. (2009), it is shown that the mesoscale and sub-mesoscale features play a role in the stratification of the water column. Seasonal and intra-seasonal variability also play a role in the MLD dynamics of the water column (Swart et al., 2015).

The temperature bias seen in the Southern Ocean, in both the Atlantic and Indian Ocean (**Figure 4.4**) correspond to the areas in which the larger northward bias is seen in the modelled STF position. This bias results in a larger SAZ due to the northward shift of the STF whilst the SAF is fairly well simulated in both models (**Figure 5.1**).

Examining the comparison of observed and modelled climatologies in **Figure 5.3,** it is evident that modelled MLD is deeper throughout the year in both the STZ and SAZ, the largest bias is present during winter. However, the modelled MLD is very well predicted in terms of seasonal variability. The MLD bias is less in the nested model due to improved vertical physics in the region of increased resolution. A study by Heuzé et al. (2015) shows that even with the increase in Argo data in recent years, the MLD in the sub-tropical Atlantic

and the Southern Ocean can still not be mapped due to insufficient data. This raises the question of whether or not the modelled MLD bias is as large as depicted in **Figure 5.3**.

High intra-seasonal variability is seen in the STZ (inside the child domain) and SAZ. The intra-seasonal variability observed in the SAZ is much higher than what is observed in the STZ. The largest difference between the models is seen in the regions of large SST and surface salinity bias (**Figure 4.4 to Figure 4.7**). A study by Swart and Speich (2010) shows that the SAZ is highly variable due to the variability of the heat and salt content in these regions; enhanced by Agulhas rings, these rings result in sudden changes in temperature and salinity. The salinity and temperature bias thus influences the MLD variability observed in the modelled data. The MLD slope is steeper throughout the deepening and restratification of the standalone MLD cycle; resulting in similar summer and spring MLD between the models. According to the correlation values (**Figure 5.5** and Table 5.1) the models simulate seasonal cycles similar to one another in areas further from the Agulhas retroflection. Higher RMSV is an indication of (**Figure 5.6**) increased vorticity (both convergent and divergent features). The magnitude of RMSV determines the strength of the vertical motion; the peaks in the nested (standalone) model precede stratification (MLD deepening) of the water column. These peaks may be a result of mesoscale eddies in the area; these features result in extreme vertical velocities (Thomas et al., 2008) and thus play an important role in the vertical structure of the water column. The improved horizontal resolution in the nested model allows for better resolved mesoscale features (Swart et al., 2015). These features play a role in the spring stratification of the water column (**Figure 5.6**), also shown in a study by Lévy et al. (2012).

The vertical structure of the water column (**Figure 5.7 to 5.18**) shows how the difference in physics, namely temperature and salinity, give rise to differences in MLD between the models. Overall the upper layer of the standalone model contains water with higher temperatures and salt content; the high density gives rise to high mechanical inertia (Palmer et al., 2015) resulting in increased turbulence. The difference between the models is highest within the child domain in the SAZ; an area with the largest local intense mixing events (Garabato et al., 2004).

On a whole this study confirms that the increased grid resolution improves the simulation of MLD. While both models capture the seasonal cycle of the domain. It is clear that a large winter bias exists in both models. This bias is less in the nested model, due to improved resolution and thus improved vertical physics. It is important to note that there are discrepancies between forcing functions which drive the model and the observed climatologies. The wind forcing used to drive the models overestimate wind speeds (Appendix A) observed over the major currents. There is no difference in wind speed between models; thus the wind speed discrepancy does not explain the MLD difference observed between models. The nested model resolves more mesoscale features, which promote stratification during spring. The BVF plots show that the water column in the nested model is overall more stratified than the standalone model water column. The larger differences between the modelled data occur within the child domain for both the STZ and the SAZ.

6.3 Summary

1. Does the increased grid resolution improve the simulation of large scale oceanographic features in the domain?
    - The models have some difficulties reproducing some oceanographic features in the Indian Ocean and the Agulhas retroflection. The flow field of the nested model is better simulated than the standalone model. Both model simulations showed that the SST and surface salinity are comparable to the observed data and to one another.

2. Does the difference in resolution result in any major oceanographic bias between models?
    - The position of the retroflection is better simulated in the nested model. The standalone model shows a weak Agulhas retroflection; the exact flow path is not clearly defined. The standalone model has a high surface temperature and salinity bias in this region.

3. Are these models able to capture MLD seasonality in the STZ and SAZ?
    - Both models are able to reproduce the general seasonal cycle in the observed climatologies. A major discrepancy in the magnitude of the MLD is seen between observed and modelled data. The models simulate MLD much deeper than the observed MLD. The bias is lesser in the nested model due to improved grid resolution in the highly variable and energetic regions of the domain.

4. How does the improved grid resolution impact the physical drivers of the MLD variability in the South Atlantic STZ and SAZ?
    - The MLD is driven mainly by temperature, salinity, mesoscale and sub-mesoscale features.
    - The improved grid resolution nested model simulates these variables with a smaller bias than that observed in the standalone model.
    - Both models can simulate mesoscale features; the nested model better simulates mesoscale features. These features allow for the smaller bias seen between observed and nested model data. The improved resolution in the nested model encourages the presence of features which promote spring stratification.
    - Overall the nested model water column is more stratified than the standalone model.

6.4 The Way Forward

- Improve numerical schemes to improve the simulations of the water masses in the Indian Ocean and the location and strength of the Agulhas system. The use of difference mixing schemes in the models may improve mixed layer dynamics.
- Use forcing functions that are more consistent with the observed climatologies when running model simulations.
- Analyse Global Earth System Models to check if the Indian Ocean water masses have been correctly simulated.

References

Antonov, J., Seidov, D., Boyer, T., Locarnini, R., Mishonov, A., Garcia, H., Baranova, O., Zweng, M. and Johnson, D. 2010. Salinity, edited by S. Levitus. *US Gov. Print. Off., Washington, DC*. World Ocean Atlas 2009, *2*: 184.

Argo Science Team. 2000. Report of the Argo Science Team 2nd Meeting (AST-2) March 7–9. Southampton Oceanography Centre, Southampton, U.K.

Beal, L.M., Chereskin, T.K., Lenn, Y.D. and Elipot, S. 2006. The sources and mixing characteristics of the Agulhas Current. *Journal of physical oceanography*, *36*(11): 2060-2074.

Billany, W., Swart, S., Hermes, J. and Reason, C.J.C., 2010. Variability of the Southern Ocean fronts at the Greenwich Meridian. *Journal of Marine Systems*, *82*(4), pp.304-310.

Boyd, P.W. 2002. Environmental factors controlling phytoplankton processes in the Southern Ocean 1. *Journal of Phycology*, *38*(5): 844-861.

Caldeira, K. and Duffy, P.B. 2000. The role of the Southern Ocean in uptake and storage of anthropogenic carbon dioxide. *Science*, *287*(5453): 620-622.

Carton, J.A. and Giese, B.S. 2008. A reanalysis of ocean climate using Simple Ocean Data Assimilation (SODA). *Monthly Weather Review*, *136*(8): 2999-3017.

Carton, J.A., Grodsky, S.A. and Liu, H. 2008. Variability of the oceanic mixed layer, 1960-2004. *Journal of Climate*, *21*(5): 1029-1047.

Casey, K.S. and Cornillon, P. 1999. A comparison of satellite and in situ-based sea surface temperature climatologies. *Journal of Climate*, *12*(6): 1848-1863.

Chu, P.C. and Fan, C. 2011. Determination of Ocean Mixed Layer Depth from Profile Data. In *Prcdgs15th Symp Int Obs Ass Sys Atmos, Ocn Lnd Sfc, AMS*: 1001-1008.

Conkright, M.E., O'Brien, T.D., Stephens, C., Locarnini, R.A., Garcia, H.E., Boyer, T.P. and Antonov, J.I. 2002. World Ocean Atlas 2001, 6, Chlorophyll.

Cronin, M.F. and Kessler, W.S. 2002. Seasonal and interannual modulation of mixed layer variability at 0, 110 W. *Deep Sea Research Part I: Oceanographic Research Papers*, *49*(1): 1-17.

de Boyer Montégut, C., Madec, G., Fischer, A.S., Lazar, A. and Iudicone, D. 2004. Mixed layer depth over the global ocean: An examination of profile data and a profile-based climatology. *Journal of Geophysical Research: Oceans*, *109*(C12).

de Ruijter, W.P., Ridderinkhof, H. and Schouten, M.W. 2005. Variability of the southwest Indian Ocean. *Philosophical Transactions of the Royal Society of London A: Mathematical, Physical and Engineering Sciences*, *363*(1826): 63-76.

de Ruijter, W.P., van Leeuwen, P.J. and Lutjeharms, J.R. 1999. Generation and evolution of Natal Pulses: solitary meanders in the Agulhas Current. *Journal of physical oceanography*, *29*(12): 3043-3055.

Deacon, G.E. 1933. A general account of the hydrology of the South Atlantic Ocean.

Durgadoo, J.V., Ansorge, I.J. and Lutjeharms, J.R. 2010. Oceanographic observations of eddies impacting the Prince Edward Islands, South Africa. *Antarctic Science*, *22*(03): 211-219.

Garabato, A.C.N., Polzin, K.L., King, B.A., Heywood, K.J. and Visbeck, M. 2004. Widespread intense turbulent mixing in the Southern Ocean. *Science*, *303*(5655): 210-213.

Garzoli, S.L. and Gordon, A.L. 1996. Origins and variability of the Benguela Current. *Journal of Geophysical Research: Oceans*, *101*(C1): 897-906.

Gill, A.E. 1982. *Atmosphere-ocean dynamics*, *30*. Academic press.

Glover, D.M., Doney, S.C., Nelson, N.B. and Wallis, A. 2008. Submesoscale anisotropy (fronts, eddies, and filaments) as observed near Bermuda with ocean color data. Paper presented at: 2008 Ocean Sciences Meeting. In *Proceedings of the 2008 Ocean Sciences Meeting*: 02-07.

Gordon, A.L., Lutjeharms, J.R. and Gründlingh, M.L. 1987. Stratification and circulation at the Agulhas Retroflection. *Deep Sea Research Part A. Oceanographic Research Papers*, *34*(4): 565-599.

Gordon, A.L., Weiss, R.A.Y.F., Smethie Jr, W.M. and Warner, M.J. 1992. Thermocline and Intermediate Water Communication. *Journal of Geophysical Research*, 97(C5): 7223-7240.

Griffies, S.M., Gnanadesikan, A.W.D.K., Dixon, K.W., Dunne, J.P., Gerdes, R., Harrison, M.J., Rosati, A., Russell, J.L., Samuels, B.L., Spelman, M.J. and Winton, M. 2005. Formulation of an ocean model for global climate simulations. *Ocean Science*, *1*(1): 45-79.

Gruber, N., Gloor, M., Mikaloff Fletcher, S.E., Doney, S.C., Dutkiewicz, S., Follows, M.J., Gerber, M., Jacobson, A.R., Joos, F., Lindsay, K. and Menemenlis, D. 2009. Oceanic sources, sinks, and transport of atmospheric CO2. *Global Biogeochemical Cycles*, *23*(1).

Heuzé, C., Vivier, F., Le Sommer, J., Molines, J.M. and Penduff, T. 2015. Can we map the interannual variability of the whole upper Southern Ocean with the current database of hydrographic observations? *Journal of Geophysical Research: Oceans*.

Höflich, O. 1984. Climate of the South Atlantic Ocean. *World survey of climatology, edited by: van Loon, H., Elsevier, Oxford*, *195*.

Hosoda, S., Ohira, T., Sato, K. and Suga, T. 2010. Improved description of global mixed-layer depth using Argo profiling floats. *Journal of oceanography*, *66*(6): 773-787.

Iwasaka, N., Kobashi, F., Kinoshita, Y. and Ohno, Y. 2006. Seasonal variations of the upper ocean in the western North Pacific observed by an Argo float. *Journal of oceanography*, *62*(4): 481-492.

Jackson, J.M., Myers, P.G. and Ianson, D. 2010. An examination of mixed layer sensitivity in the northeast Pacific Ocean from July 2001–July 2005 using the general ocean turbulence model and Argo data. *Atmosphere-ocean*, *47*(2): 139-153.

Joubert, W.R., Swart, S., Tagliabue, A., Thomalla, S.J. and Monteiro, P.M.S. 2014. The sensitivity of primary productivity to intra-seasonal mixed layer variability in the sub-Antarctic Zone of the Atlantic Ocean. *Biogeosciences Discussions*, *11*(3): 4335-4358.

Juza, M., Penduff, T., Brankart, J.M. and Barnier, B. 2012. Estimating the distortion of mixed layer property distributions induced by the Argo sampling.*Journal of Operational Oceanography*, *5*(1): 45-58.

Kara, A.B., Rochford, P.A. and Hurlburt, H.E. 2000. Mixed layer depth variability and barrier layer formation over the North Pacific Ocean. *Journal of Geophysical Research: Oceans*, *105*(C7): 16783-16801.

Lalli, C. and Parsons, T.R. 1995. *Biological Oceanography: An Introduction: An Introduction*. Butterworth-Heinemann.

Lenton, A., Tilbrook, B., Law, R., Bakker, D., Doney, S.C., Gruber, N., Hoppema, M., Ishii, M., Lovenduski, N.S., Matear, R.J. and McNeil, B.I. 2013. Sea-air CO2 fluxes in the Southern Ocean for the period 1990–2009. *Biogeosciences Discussions*, *10*: 285-333.

Lévy, M. 2008. The modulation of biological production by oceanic mesoscale turbulence. In *Transport and Mixing in Geophysical Flows*. Springer Berlin Heidelberg: 219-261.

Lévy, M., Ferrari, R., Franks, P.J., Martin, A.P. and Rivière, P. 2012. Bringing physics to life at the submesoscale. *Geophysical Research Letters*, *39*(14).

Lévy, M., Klein, P. and Treguier, A.M. 2001. Impact of sub-mesoscale physics on production and subduction of phytoplankton in an oligotrophic regime. *Journal of marine research*, *59*(4): 535-565.

Loveday, B. 2014. Multi-tier Inter-regional Model of Southern Africa (MIMOSA), Untitled report. University of Cape Town.

Loveday, B.R., Penven, P. and Reason, C.J.C., 2015. Southern Annular Mode and westerly-wind-driven changes in Indian-Atlantic exchange mechanisms. *Geophysical Research Letters*, *42*(12), pp.4912-4921.

Lutjeharms, J.R. (2006). The Agulhas current. Berlin : Springer.

Lutjeharms, J.R.E. and Gordon, A.L. 1987. Shedding of an Agulhas ring observed at sea. *Nature*, *325*(6100): 138-140.

Lutjeharms, J.R.E. and Van Ballegooyen, R.C. 1988. The retroflection of the Agulhas Current. *Journal of Physical Oceanography*, *18*(11): 1570-1583.

McKiver, W.J., Vichi, M., Lovato, T., Storto, A. and Masina, S. 2015. Impact of increased grid resolution on global marine biogeochemistry. *Journal of Marine Systems*, *147:* 153-168.

Meeuwis, J.M. and Lutjeharms, J.R.E. 1990. Surface thermal characteristics of the Angola-Benguela front. *South African Journal of Marine Science*, *9*(1): 261-279.

Meijers, A.J.S. 2014. The Southern Ocean in the Nested Model Intercomparison Project phase 5. *Philosophical Transactions of the Royal Society of London A: Mathematical, Physical and Engineering Sciences*, *372*(2019): 20130296.

Mercier, H., Arhan, M. and Lutjeharms, J.R. 2003. Upper-layer circulation in the eastern Equatorial and South Atlantic Ocean in January–March 1995.*Deep Sea Research Part I: Oceanographic Research Papers*, *50*(7): 863-887.

Moigne, F.L., Boye, M., Masson, A., Corvaisier, R., Grossteffan, E., Guéneugues, A. and Pondaven, P. 2012. Description of the biogeochemical features of the subtropical southeastern Atlantic and the Southern Ocean south off South Africa during the austral summer of the International Polar Year. *Biogeosciences Discussions*, *9*(4): 5011.

Momin, I.M., Mitra, A.K., Mahapatra, D.K., Gera, A. and Rajagopal, E.N. 2014. Impact of model resolutions on Indian ocean simulations from Global NEMO Ocean Model. *Indian Journal of Geo-Marine Science*, *43:* 9.

Monteiro, P., Boyd, P. and Bellerby, R. 2011. Role of the seasonal cycle in coupling climate and carbon cycling in the Subantarctic zone. *Eos, Transactions American Geophysical Union*, *92*(28): 235-236.

Nowlin Jr, W.D., Whitworth III, T. and Pillsbury, R.D. 1977. Structure and transport of the Antarctic Circumpolar Current at Drake Passage from short-term measurements. *Journal of Physical Oceanography*, *7*(6): 788-802.

Orsi, A.H., Whitworth, T. and Nowlin, W.D. 1995. On the meridional extent and fronts of the Antarctic Circumpolar Current. *Deep Sea Research Part I: Oceanographic Research Papers*, *42*(5): 641-673.

Otobe, H., Taira, K., Kitagawa, S., Asai, T. and Hanawa, K. 2003. Variability of upper ocean heat balance in the Shikoku Basin during the Ocean Mixed Layer Experiment (OMLET). *Journal of oceanography*, *59*(5): 619-627.

Palmer, M.R., Stephenson, G.R., Inall, M.E., Balfour, C., Düsterhus, A. and Green, J.A.M. 2015. Turbulence and mixing by internal waves in the Celtic Sea determined from ocean glider microstructure measurements. *Journal of Marine Systems*, *144*: 57-69.

Park, Y.H., Gamberoni, L. and Charriaud, E. 1993. Frontal structure, water masses, and circulation in the Crozet Basin. *Journal of Geophysical Research: Oceans*, *98*(C7): 12361-12385.

Penduff, T., Juza, M. and Barnier, B. 2007. Assessing the realism of ocean simulations against hydrography and altimetry. *Clivar Exchanges*, *12*(3): 11-12.

Penven, P., Marchesiello, P., Debreu, L. and Lefevre, J. 2008. Software tools for pre-and post-processing of oceanic regional simulations.*Environmental Modelling & Software*, *23*(5): 660-662.

Peterson, R.G. and Stramma, L. 1991. Upper-level circulation in the South Atlantic Ocean. *Progress in oceanography*, *26*(1): 1-73.

Rintoul, S.R. 1991. South Atlantic interbasin exchange. *Journal of Geophysical Research: Oceans*, *96*(C2): 2675-2692.

Rio, M.H., Guinehut, S. and Larnicol, G. 2011. New CNES-CLS09 global mean dynamic topography computed from the combination of GRACE data, altimetry, and in situ measurements. *Journal of Geophysical Research: Oceans* (1978–2012), 116(C7).

Roemmich, D. 1983. "The balance of geostrophic and Ekman transports in the tropical Atlantic Ocean." *Journal of Physical Oceanography* 13.8: 1534-1539.

Saha, S., Moorthi, S., Pan, H.L., Wu, X., Wang, J., Nadiga, S., Tripp, P., Kistler, R., Woollen, J., Behringer, D. and Liu, H. 2010. NCEP Climate Forecast System Reanalysis (CFSR) 6-hourly Products, January 1979 to December 2010. *Research Data, The National Center for Atmospheric Research, Computational and Information Systems Laboratory, Boulder, Colo, USA*.

Shchepetkin, A.F. and McWilliams, J.C. 2005. The regional oceanic modeling system (ROMS): a split-explicit, free-surface, topography-following-coordinate oceanic model. *Ocean Modelling*, *9*(4): 347-404.

Schlitzer, R. 2002. Carbon export fluxes in the Southern Ocean: results from inverse modeling and comparison with satellite-based estimates. *Deep Sea Research Part II: Topical Studies in Oceanography*, *49*(9): 1623-1644.

Schonten, M.W., Ruijter, W.P., Leeuwen, P.J. and Lutjeharms, J.R. 2000. Translation, decay and splitting of Agulhas rings in the southeastern Atlantic Ocean. *Journal of Geophysical Research: Oceans*, *105*(C9): 21913-21925.

Schott, F.A., Xie, S.P. and McCreary, J.P., 2009. Indian Ocean circulation and climate variability. *Reviews of Geophysics*, *47*(1).

Sokolov, S. and Rintoul, S.R. 2002. Structure of Southern Ocean fronts at 140 E. *Journal of Marine Systems*, *37*(1): 151-184.

Stramma, L. and Lutjeharms, J.R. 1997. The flow field of the subtropical gyre of the South Indian Ocean. *Journal of Geophysical Research: Oceans*, *102*(C3): 5513-5530.

Stramma, L. and Peterson, R.G. 1990. The South Atlantic Current. *Journal of Physical Oceanography*, *20*(6): 846-859.

Swart, S. and Speich, S. 2010. An altimetry-based gravest empirical mode south of Africa: 2. Dynamic nature of the Antarctic Circumpolar Current fronts. *Journal of Geophysical Research: Oceans*, *115*(C3).

Swart, S., Speich, S., Ansorge, I.J., Goni, G.J., Gladyshev, S. and Lutjeharms, J.R. 2008. Transport and variability of the Antarctic Circumpolar Current south of Africa. *Journal of Geophysical Research: Oceans*, *113*(C9).

Swart, S., Thomalla, S.J. and Monteiro, P.M.S. 2015. The seasonal cycle of mixed layer dynamics and phytoplankton biomass in the Sub-Antarctic Zone: A high-resolution glider experiment. *Journal of Marine Systems*, *147*: 103-115.

Talley, L.D. 2011. *Descriptive physical oceanography: an introduction*. Academic press.

Thomalla, S.J., Fauchereau, N., Swart, S. and Monteiro, P.M.S. 2011. Regional scale characteristics of the seasonal cycle of chlorophyll in the Southern Ocean. *Biogeosciences*, *8*(10): 2849-2866.

Thomas, L.N. 2005. Destruction of potential vorticity by winds. *Journal of Physical Oceanography*, *35*(12): 2457-2466.

Thomson, R.E. and Fine, I.V. 2003. Estimating mixed layer depth from oceanic profile data. *Journal of Atmospheric and Oceanic Technology*, *20*(2): 319-329.

Tomczak, M. and Godfrey, J.S. 2013. *Regional oceanography: an introduction*. Elsevier.

Trenberth, K.E., Large, W.G. and Olson, J.G. 1990. The mean annual cycle in global ocean wind stress. *Journal of Physical Oceanography*, *20*(11): 1742-1760.

U.S. Department of Commerce, National Oceanic and Atmospheric Administration, National Geophysical Data Center. 2006. *2-minute Gridded Global Relief Data (ETOPO2v2)* http://www.ngdc.noaa.gov/mgg/fliers/06mgg01.html

van Sebille, E., Biastoch, A., Van Leeuwen, P.J. and De Ruijter, W.P.M. 2009. A weaker Agulhas Current leads to more Agulhas leakage.*Geophysical Research Letters*, *36*(3).

Veronis, G. 1973. MODEL OF WORLD OCEAN CIRCULATION. 1. WIND-DRIVEN, 2-LAYER. *Journal of Marine Research*, *31*(3): 228-288.

Vichi, M. and Masina, S. 2009. Skill assessment of the PELAGOS global ocean biogeochemistry model over the period 1980–2000. *Biogeosciences*, *6*(11): 2333-2353.

Vichi, M., Masina, S. and Navarra, A. 2007. A generalized model of pelagic biogeochemistry for the global ocean ecosystem. Part II: Numerical simulations. *Journal of Marine Systems*, *64*(1): 110-134.

Walker, N.D. 1989. Sea-surface temperature-rainfall relationships and associated ocean-atmosphere coupling mechanisms in the southern African region. Ph.D. thesis of the University of Cape Town.

Warner, J.C., Sherwood, C.R., Arango, H.G. and Signell, R.P., 2005. Performance of four turbulence closure models implemented using a generic length scale method. *Ocean Modelling*, *8*(1), pp.81-113.

Whitworth, T. and Nowlin, W.D. 1987. Water masses and currents of the Southern Ocean at the Greenwich Meridian. *Journal of Geophysical Research: Oceans*, *92*(C6): 6462-6476.

Wyrtki, K. 1971. Oceanographic atlas of the international Indian Ocean expedition. National Science Foundation.

APPENDIX A

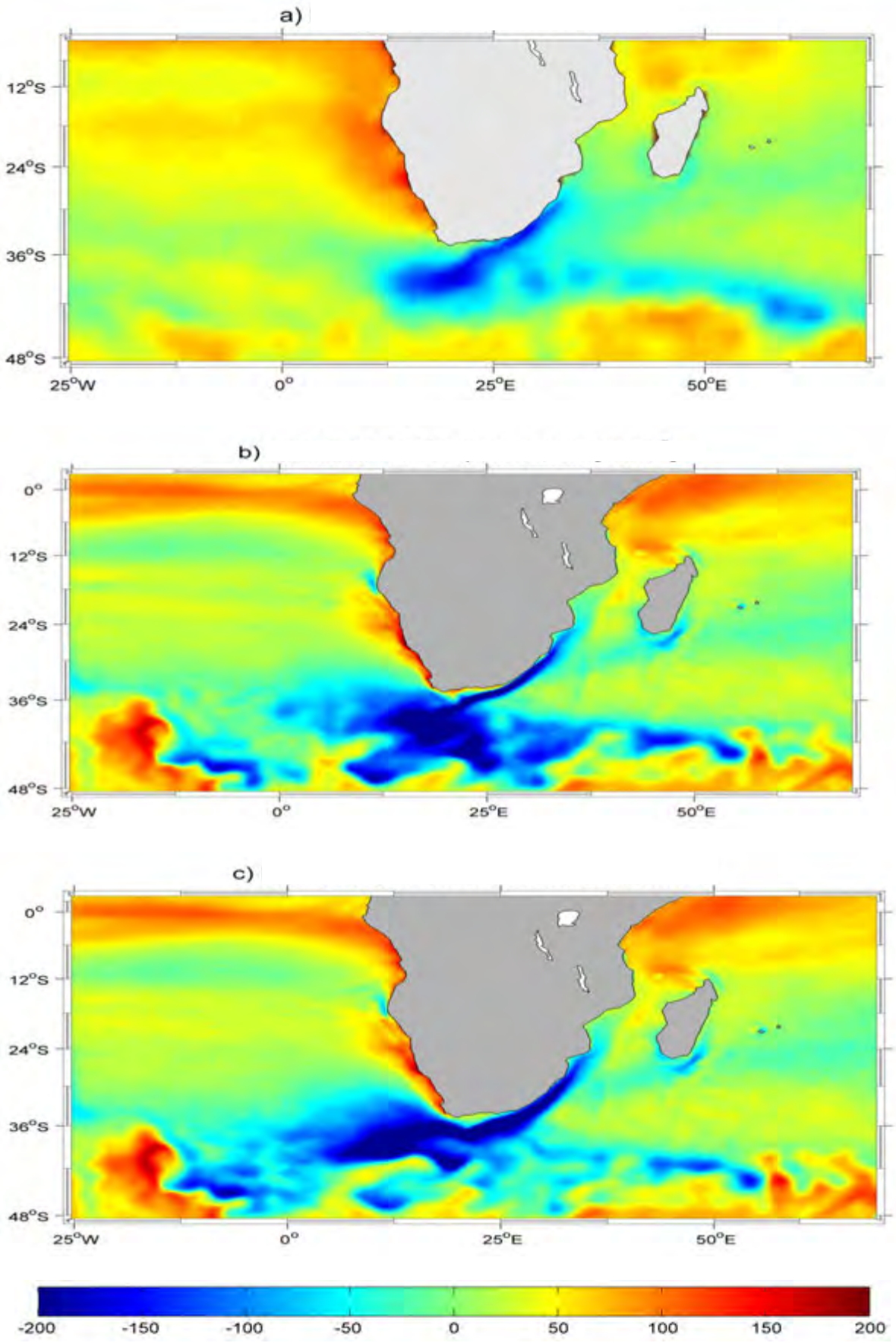

Figure 1 Mean surface net heat flux in the domain. a) Heat flux for OAFLUX data, b) Heat flux for nested model data and c) Heat flux for standalone model data.

APPENDIX A

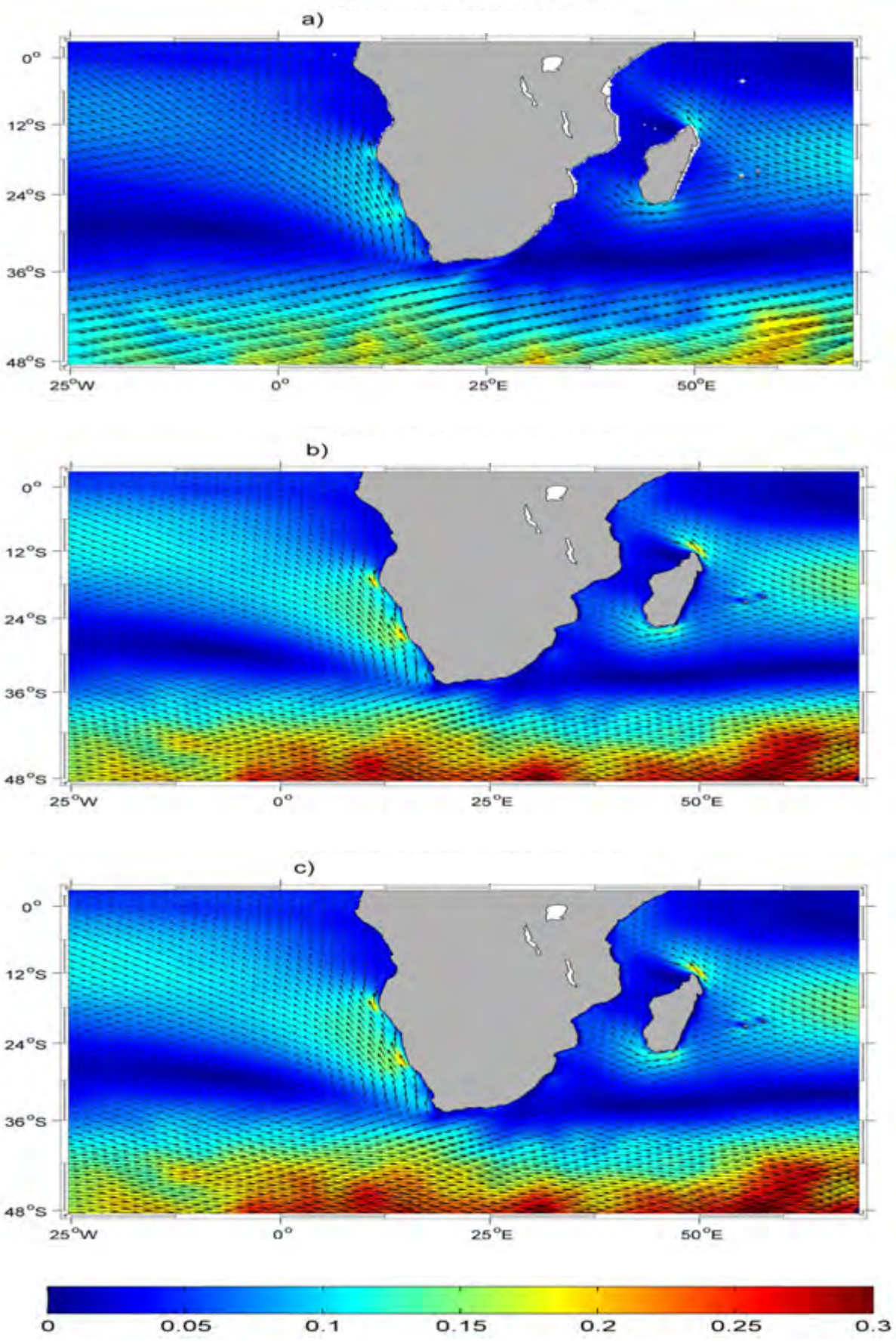

Figure 2 Mean surface wind speed (m/s) and direction. The arrows indicate the direction of the wind and the colour indicated the speed of the wind in the domain. a) Wind for QuikSCAT data, b) Wind of nested model data and c) Wind of Standalone model data.